JHEP

Published for SISSA by Springer

Received: November 23, 2020
Accepted: January 25, 2021
Published: March 9, 2021

Two and three pseudoscalar production in e^+e^- annihilation and their contributions to $(g-2)_\mu$

Wen Qin,[a,b] **Ling-Yun Dai**[a,b] **and Jorge Portolés**[c]

[a] *School of Physics and Electronics, Hunan University, Changsha 410082, China*
[b] *Hunan Provincial Key Laboratory of High-Energy Scale Physics and Applications, Hunan University, Changsha 410082, China*
[c] *IFIC, CSIC — Universitat de València, Apt. Correus 22085, E-46071 València, Spain*

E-mail: wqin@hnu.edu.cn, dailingyun@hnu.edu.cn, Jorge.Portoles@ific.uv.es

Abstract: A coherent study of e^+e^- annihilation into two ($\pi^+\pi^-$,K^+K^-) and three ($\pi^+\pi^-\pi^0, \pi^+\pi^-\eta$) pseudoscalar meson production is carried out within the framework of resonance chiral theory in energy region $E \lesssim 2\,\text{GeV}$. The work of [L.Y. Dai, J. Portolés, and O. Shekhovtsova, *Phys. Rev. D* **88** (2013) 056001] is revisited with the latest experimental data and a joint analysis of two pseudoscalar meson production. Hence, we evaluate the lowest order hadronic vacuum polarization contributions of those two and three pseudoscalar processes to the anomalous magnetic moment of the muon. We also estimate some higher-order additions led by the same hadronic vacuum polarization. Combined with the other contributions from the standard model, the theoretical prediction differs still by $(21.6 \pm 7.4) \times 10^{-10}$ (2.9σ) from the experimental value.

Keywords: Phenomenological Models, QCD Phenomenology

ArXiv ePrint: 2011.09618

https://doi.org/10.1007/JHEP03(2021)092

JHEP03(2021)092

Contents

JHEP03(2021)092

1 Introduction

It is well known that Quantum Chromodynamics (QCD) is successful in describing strong interactions. In the high energy region, the correlation functions could be well determined by perturbative QCD. However, the situation becomes more complicated in the low energy region, as the strong coupling constant increases when the energy decreases. Fortunately, at the very low energy region $E \ll M_\rho$ [M_ρ being the mass of the $\rho(770)$], the spontaneous chiral symmetry breaking of QCD generates the pseudoscalar octet of Goldstone bosons, which are treated as degrees of freedom in the effective field theory (EFT) of QCD: chiral perturbation theory (χPT) [1, 2]. However, χPT is not the EFT in the intermediate energy region, $M_\rho \lesssim E \lesssim 2\,\text{GeV}$, where it is populated by dense spectra of resonances. Resonance chiral theory (RχT) is a reasonable approach to extent the working regime of χPT by including the resonances as new degrees of freedom [3–6]. The construction of the lagrangian is guided by Lorentz invariance and by chiral and discrete symmetries, i.e. C-, P-parity conservation. The lack of a coupling that may guide a perturbative expansion in the calculations of the amplitudes, is compensated by a model of the large-N_C setting (being N_C the number of colours) [7–9]. As in χPT, this approach produces the relevant operators in the lagrangian, in terms of Goldstone bosons, resonances and external fields, but leaves undetermined their coupling constants.

One may use experimental data to obtain information of the couplings. Meanwhile, there is one theoretical tool that has proven efficient in this task: one can extract information on the coupling constants by matching the perturbative Green functions of QCD currents, using the operator product expansion (OPE) at leading order, with those constructed in the RχT framework [10–16]. Actually, RχT can also match, by construction, with χPT by integrating out the resonances in the Lagrangian [4, 17], allowing to relate their coupling constants, too. Indeed RχT is successful in dealing with the lightest resonances and their interaction with the lightest pseudoscalars. It has been well applied in the study of hadron tau decays [18–24], two-photon transition form factors [25–27], and e^+e^- annihilation in the nonperturbative regime of QCD [28, 29].

Low-energy processes with many hadrons in the final state involve final-state interactions (FSI) that are notoriously difficult to deal with in a model independent way. The use of dispersive approaches to deal with them is possible in some instances, namely when good phenomenological data are available (see for instance refs. [30–36] for some recent work). In the framework of RχT, this is also achievable as we did in ref. [29], where both vector-meson dominance and the anomalous terms were considered in a coherent analysis of the $e^+e^- \to \pi^+\pi^-\pi^0, \pi^+\pi^-\eta$ channels, in the energy region populated by many hadron resonances up to $E \lesssim 2.3\,\text{GeV}$. Here we will revisit that work and extend it to two pseudoscalar production in the light of the new data.

Recent interest on e^+e^- annihilation into two and three pesudoscalars is driven by their contribution to the anomalous magnetic moment of the muon $a_\mu = (g_\mu - 2)/2$, with g_μ the muon Landé factor. The theoretical prediction of a_μ has become a major tour de force in the last years because, on the experimental side, it has been measured with high precision, $a_\mu^{\text{exp}} = 11659208.9(6.3) \times 10^{-10}$ [37, 38], and there seems to be a $3.3\,\sigma$ [38] or $3.7\,\sigma$ [39] discrepancy from the standard model (SM) prediction. This fact paves the possibility of bringing out new physics contributions. Within the standard model [39, 40], the most important contribution, the electromagnetic one, is accurately calculated up to tenth-order α_e^5, $a_\mu^{\text{QED}} = 11658471.8931(104) \times 10^{-10}$, with very small uncertainty [41, 42]. The electroweak contribution at the two-loop level is also well determined as $a_\mu^{\text{EW}} = 15.36(0.1) \times 10^{-10}$ [43–46]. The hadronic contribution is considered as the major source of uncertainty and has two components: hadronic light-by-light scattering (HLBL) and hadronic vacuum polarization (HVP). The HLBL cannot be directly estimated from experimental input, and a combination of different theoretical models has estimated it as $a_\mu^{\text{HLBL}} = 9.2(1.8) \times 10^{-10}$ [39, 47–49]. The lattice calculations on HLBL and HVP can be found in, e.g. refs. [50–53]. A comprehensive amplitude analysis on $\gamma\gamma \to \pi\pi, K\bar{K}$ is done in refs. [54–57]. They are indeed the constraints on HLBL where the photons are real. HVP is the largest hadronic contribution and it is related with the cross section of $e^+e^- \to$ anything throughout causality and unitarity.[1] The present value for the leading order HVP contribution is $a_\mu^{\text{HVP,LO}} = 694.0(4.0) \times 10^{-10}$ [60]. And the next-to-leading order and next-to-next-to-leading order HVP corrections are derived by considering also higher order hadronic loops, $a_\mu^{\text{HVP,NLO}} = -9.83(0.07) \times 10^{-10}$ [61], $a_\mu^{\text{HVP,NNLO}} = 1.24(0.01) \times 10^{-10}$ [62]. The com-

[1] We note that in the early works [58, 59], the upper limit of HVP contribution has been given.

JHEP03(2021)092

putation of the HVP contribution relies heavily on the available experimental data and, consequently, its improvement will come from the accurate measurement of the electron-positron cross-section.

Comparing the theoretical predictions from the SM with the experimental measurement, there is still a discrepancy, as commented above. There are lots of experimental data available. However, there are discordances among different collaborations, even those with the highest statistics datasets. The study of three pseudoscalar production was carried out in ref. [29], but recently new experimental measurements of $e^+e^- \to \pi^+\pi^-\pi^0, \pi^+\pi^-\eta$ have become available. SND [63] has given a new measurement of $e^+e^- \to \pi^+\pi^-\pi^0$ in the energy range $1.05 - 2.00\,\text{GeV}$. BESIII [64] provided a measurement for $e^+e^- \to \pi^+\pi^-\pi^0$ in a wide energy range between 0.7 and 3.0 GeV using the Initial State Radiation (ISR) method. SND also measured $e^+e^- \to \eta\pi\pi$ channel with η in $\eta \to \gamma\gamma$ mode [65] and $\eta \to 3\pi^0$ mode [66], and a combined results of these two modes were provided in [66]. CMD3 [67] also measured $e^+e^- \to \eta\pi\pi$ in $\eta \to \gamma\gamma$ mode, and the cross section values combined with its previous measurements were provided. Very recently, BESIII measured $e^+e^- \to \eta'\pi\pi$ above 2 GeV [68]. Besides, there are also new experimental measurements for the two pseudoscalar cases. BaBar [69] measured $e^+e^- \to \pi^+\pi^-$ from threshold up to 3 GeV. KLOE has done three precise measurements of $e^+e^- \to \pi^+\pi^-$ [70–72], using ISR below 1 GeV, and a combined results with all these three measurements were provided in ref. [73]. There are also precise measurements below 1 GeV, such as, SND [74], BESIII [75] and CLEO [76]. Before 2008, there are also lots of experiment datasets, CMD2 [77–79], DM2 [80] and CMD & OLYA [81]. In contrast, the $e^+e^- \to K^+K^-$ process has a considerably shorter history starting from SND [82] in 2001. Later, SND updated the measurements in 2007 [83], and the most recently one in 2016 [84]. In 2019, a high precision measurement has been given by BESIII [85]. There are also some other measurements from BarBar [86], CMD2 [87] and CMD3 [88].

In this paper, we give a coherent analysis of e^+e^- annihilation into two pseudoscalars $\pi^+\pi^-$,K^+K^- and three pseudoscalars $\pi^+\pi^-\pi^0, \pi^+\pi^-\eta$ based on the former work [29], combined with all the recent experimental measurements. In section 2 we will briefly update the theoretical framework and give the amplitudes calculated by RχT. In section 3, we fit the amplitudes to the experimental data up to 2.3 GeV. In section 4, the leading order HVP contribution to $g-2$ is estimated. Higher-order hadronic contributions are considered in section 5. Finally, we collect our conclusions in section 6. An appendix collects detailed expressions for the involved form factors and decay widths.

2 Theoretical framework updates and notations

2.1 RχT and further improvements on the form factors

Massless QCD exhibits a chiral symmetry that rules its effective field theory at low energy. χPT, valid at $E \ll M_\rho$, provides the interaction between the lightest octet of pseudoscalar mesons, and of these with external currents. At higher energies we need to take into account the hadronic resonance states, and a successful phenomenological approach is provided by

JHEP03(2021)092

RχT, which aspects of interest for our case we briefly collect here. We follow the language and notation of ref. [5].

The structure of the lagrangian has, essentially, three pieces:

$$\mathcal{L}_{\mathrm{R}\chi\mathrm{T}} \,=\, \mathcal{L}_{\mathrm{GB}} \,+\, \mathcal{L}^{\mathrm{V}}_{\mathrm{kin}} \,+\, \mathcal{L}_{\mathrm{V-GB}}\,. \tag{2.1}$$

The first piece involves interaction terms with Goldstone bosons that cannot be generated by integrating out the vector resonance states. They are characterized by a perturbative expansion in terms of momenta (and masses), as in χPT. $\mathcal{L}^{\mathrm{V}}_{\mathrm{kin}}$ involves the kinetic term of the vector resonance states and $\mathcal{L}_{\mathrm{V-GB}}$ the interaction between Goldstone bosons and vector resonance fields. For the processes that we study in this work only the vector resonance fields will be needed. All of these lagrangians include also external fields coupled to scalar, pseudoscalar, vector, axial-vector or tensor currents. The lowest even-intrinsic-parity $\mathcal{O}(p^2)$ of the $\mathcal{L}_{\mathrm{GB}}$ Lagrangian is given by

$$\mathcal{L}^{\mathrm{GB}}_{(2)} \equiv \mathcal{L}^{\chi\mathrm{PT}}_{(2)} = \frac{F^2}{4}\left\langle u_\mu u^\mu + \chi_+ \right\rangle\,, \tag{2.2}$$

being F the decay constant of the pion and $\langle\ldots\rangle$ indicates the trace in the SU(3) space. The leading Wess-Zumino-Witten term describing the anomaly with odd-intrinsic-parity is of $\mathcal{O}(p^4)$ [89, 90]. The explicit expression of interest for our work is given by

$$\mathcal{L}^{\mathrm{GB}}_{(4)} \,=\, i\frac{N_C\sqrt{2}}{12\pi^2F^3}\,\varepsilon_{\mu\nu\rho\sigma}\,\left\langle \partial^\mu\Phi\partial^\nu\Phi\partial^\rho\Phi v^\sigma\right\rangle + \cdots\,, \tag{2.3}$$

where v^σ is the external vector current and Φ the multiplet of Goldstone bosons. Higher orders of the $\mathcal{L}_{\mathrm{GB}}$ lagrangian will not be considered, as we assume that their couplings are dominated by resonance contributions.[2]

The kinetic term of the vector resonance field is given by

$$\mathcal{L}^{\mathrm{V}}_{\mathrm{kin}} = -\frac{1}{2}\left\langle \nabla^\lambda V_{\lambda\mu}\nabla_\nu V^{\nu\mu}\right\rangle + \frac{1}{4}M_V^2\left\langle V_{\mu\nu}V^{\mu\nu}\right\rangle\,, \tag{2.4}$$

Here the resonances are collected as $\mathrm{SU}(3)_V$ octets and have the corresponding properties under chiral transformations. The Lagrangian that involves the interaction between Goldstone bosons and vector resonances, $\mathcal{L}_{\mathrm{V-GB}}$, couples the later octets with a chiral tensor constituted by the pseudoscalar nonet and external fields. Hence these chiral tensors obey a chiral counting $\mathcal{O}(p^n)$. This allows us to assign a label n to the different pieces as $\mathcal{L}^{V\cdots}_{(n)}$, where the numerator indicates the resonance fields in the interaction terms. We will consider

$$\mathcal{L}_{\mathrm{V-GB}} = \mathcal{L}^{\mathrm{V}}_{(2)} + \mathcal{L}^{\mathrm{V}}_{(4)} + \mathcal{L}^{\mathrm{VV}}_{(2)}\,. \tag{2.5}$$

For instance, in the antisymmetric formulation for the spin-one vector resonances that we use,

$$\begin{aligned}\mathcal{L}^{\mathrm{V}}_{(2)} &= \left\langle\, V_{\mu\nu}\,\chi^{\mu\nu}_{(2)}\,\right\rangle,\\ \chi^{\mu\nu}_{(2)} &= \frac{F_V}{2\sqrt{2}}\,f_+^{\mu\nu} \,+\, i\,\frac{G_V}{\sqrt{2}}\,u^\mu\,u^\nu\end{aligned} \tag{2.6}$$

[2] Up to $\mathcal{O}(p^4)$ at least, this setting depends on the realization of the spin-1 resonance fields. In ref. [4], it was proven that this assumption is correct if one uses the antisymmetric formulation for those fields, as we do.

JHEP03(2021)092

where F_V and G_V are coupling constants not determined by the symmetry. The rest of terms in eq. (2.5) are collected in ref. [5] for the even-intrinsic-parity terms and refs. [11, 19, 29] for those of odd-intrinsic parity. The coupling constants of the interaction terms of $\mathcal{L}_{\rm V-GB}$ could be extracted from the phenomenology involving those states. As commented in the introduction the matching between the leading order in the OPE expansion of specific Green functions of QCD and their expressions within RχT is also a useful tool that has been employed in the bibliography [10–16]. We will implement this procedure as far as it helps in our task. In particular we will use the relations between couplings specified in ref. [29].

However, the large energy region of study cannot be described fully with only one multiplet of vector resonances $V_{\mu\nu}$. The lightest one is situated around M_ρ, i.e. under 1 GeV. Two other vector multiplets populate the interval $1\,\text{GeV} \lesssim E \lesssim 2\,\text{GeV}$, that we will call $V'_{\mu\nu}$ and $V''_{\mu\nu}$. Their couplings to the pseudoscalar mesons will be defined with respect to the ones of the lightest multiplet as $\beta'_{\pi\pi}$,$\beta''_{\pi\pi}$,β'_{KK},β''_{KK}, through their poles, as

$$\frac{1}{M_V^2-x} \to \frac{1}{M_V^2-x} + \frac{\beta'_{\pi\pi,KK}}{M_{V'}^2-x} + \frac{\beta''_{\pi\pi,KK}}{M_{V''}^2-x}\ . \tag{2.7}$$

The $\rho-\omega$ mixing, required by the $e^+e^- \to \pi^+\pi^-$ process, is reconsidered. While a constant mixing angle δ_0 is enough to describe mixing in the three pseudoscalar case as discussed in ref. [29]:

$$\begin{pmatrix} |\bar\rho^0\rangle \\ |\bar\omega\rangle \end{pmatrix} = \begin{pmatrix} \cos\delta_0 & -\sin\delta_0 \\ \sin\delta_0 & \cos\delta_0 \end{pmatrix} \begin{pmatrix} |\rho^0\rangle \\ |\omega\rangle \end{pmatrix}\ , \tag{2.8}$$

an energy dependent mixing angle is discussed in ref. [91], although in the non-relativistic limit and we need to generalize it to the relativistic case. The energy dependent mixing angle could be parameterized as

$$\begin{aligned} \begin{pmatrix} |\bar\rho^0\rangle \\ |\bar\omega\rangle \end{pmatrix} &= \begin{pmatrix} \cos\delta & \frac{M_V\Gamma_\rho \sin\delta}{-(M_V^2-s)+iM_V(\Gamma_\rho-\Gamma_\omega)} \\ \frac{M_V\Gamma_\rho \sin\delta}{-(M_V^2-s)-iM_V(\Gamma_\rho-\Gamma_\omega)} & \cos\delta \end{pmatrix} \begin{pmatrix} |\rho^0\rangle \\ |\omega\rangle \end{pmatrix} \\ &\equiv \begin{pmatrix} \cos\delta & -\sin\delta^\omega(s) \\ \sin\delta^\rho(s) & \cos\delta \end{pmatrix} \begin{pmatrix} |\rho^0\rangle \\ |\omega\rangle \end{pmatrix}\ , \end{aligned} \tag{2.9}$$

where $|\rho^0\rangle\,, |\omega\rangle$ denote the physical states. Hence the energy dependence of the mixing angle is driven by the resonance propagators. Here M_V is the mass of the nonet of vector resonances in the SU(3) limit. We will take $M_V = M_\rho$. For the two body final state processes $e^+e^- \to \pi^+\pi^-, K^+K^-$, we always take energy dependent mixing mechanism according to eq. (2.9). For the three body cases, we adopt two ways. One is to take the same energy dependent $\rho-\omega$ mixing mechanism as that of the two body case. This will be Fit I. The other is to use the constant mixing angle δ_0. This will be our Fit II. Comparison of both fits will unveil the influence of $\rho-\omega$ mixing in the analysis of data.

2.2 Cross sections for two and three pseudoscalar final states

The amplitude for three-meson production in e^+e^- collisions is driven by the hadronization of the electromagnetic current, in terms of one vector form factor only:

$$\langle \pi^+(p_1)\pi^-(p_2)P(p_3)|\left(\mathcal{V}_\mu^3 + \mathcal{V}_\mu^8/\sqrt{3}\right) e^{i\mathcal{L}_{\rm QCD}}|0\rangle \ = \ i\,F_V^P(Q^2,s,t)\,\varepsilon_{\mu\nu\alpha\beta}\,p_1^\nu p_2^\alpha p_3^\beta\,, \tag{2.10}$$

JHEP03(2021)092

being $\mathcal{V}^i_\mu = \bar{q}\gamma_\mu(\lambda^i/2)q$ and $P = \pi, \eta$. The Mandelstam variables are defined as $s = (Q - p_3)^2$, $t = (Q - p_1)^2$, with $Q = p_1 + p_2 + p_3$. The cross section and amplitudes for the three pseudoscalar cases that we are considering, namely $e^+e^- \to \pi^+\pi^-\pi^0$ and $e^+e^- \to \pi^+\pi^-\eta$, are quite the same as specified in ref. [29], except for a small change in the treatment of $\rho - \omega$ mixing, as illustrated in section 2.1. The corresponding expressions for the cross-section and the modified form factors for the three pseudoscalar cases are collected in appendix A.

These form factors depend on several couplings of the RχT lagrangian that are not determined by the symmetry. However, some of them or, at least, relations between them can be established by matching Green functions calculated in this framework with their expressions at leading order OPE expansion of QCD, as it has been commented before. By implementing these short-distance relations our form factors satisfy both the chiral constraints in the low-energy region and the asymptotic constraints at the high energy limit ($Q^2 \to \infty$). Hence the only unknown couplings in these form factors will be F_V, $2g_4 + g_5$, d_2, c_3 and α_V [29], to be added to the $\beta'_{\pi\pi,KK}$ and $\beta''_{\pi\pi,KK}$ from eq. (2.7) and the mixing angles between the octet and singlet pseudoscalar (θ_P) and vector (θ_V) components, defined also in [29].

Two-pseudoscalar final states in e^+e^- annihilation are given by the corresponding vector form factor

$$\langle P^+(p_1)P^-(p_2)|\left(\mathcal{V}^3_\mu + \mathcal{V}^8_\mu/\sqrt{3}\right) e^{i\mathcal{L}_{\rm QCD}}|0\rangle = (p_1 - p_2)_\mu F_V^P(Q^2)\,, \tag{2.11}$$

with $Q = p_1 + p_2$ and $P = \pi, K$. The energy in the center of mass frame is given by $E_{cm} \equiv \sqrt{Q^2}$. The cross sections $\sigma_{\pi\pi} \equiv \sigma(e^+e^- \to \pi^+\pi^-)$ and $\sigma_{KK} \equiv \sigma(e^+e^- \to K^+K^-)$ are given by

$$\sigma_{PP} = \alpha_e^2 \frac{\pi}{3\,Q^2}\left(1 - 4\frac{m_P^2}{Q^2}\right)^{3/2} |F_V^P(Q^2)|^2\,. \tag{2.12}$$

The form factors $F_V^\pi(Q^2)$ and $F_V^K(Q^2)$ were thoroughly studied in ref. [92] (see also [93–95] for alternative parameterizations) in the case of tau decays. Hence we need to include now the new $\rho - \omega$ mixing mechanism, present in e^+e^- into hadrons. We also extend the described energy region by adding heavier vector multiplets, as commented above. Their expressions are:

$$\begin{aligned} F_V^\pi = &\left(1 + \frac{F_V G_V}{F^2} Q^2 \left(BW(M_\rho, \Gamma_{\rho,}, Q^2) + \beta'_{\pi\pi} BW(M_{\rho'}, \Gamma_{\rho'}, Q^2)\right.\right. \\ &\left. + \beta''_{\pi\pi} BW(M_{\rho''}, \Gamma_{\rho''}, Q^2)\right)\left(\frac{1}{\sqrt{3}}\sin\theta_V \sin\delta^\rho + \cos\delta\right)\cos\delta \\ &- \frac{F_V G_V}{F^2} Q^2 \left(BW(M_\omega, \Gamma_{\omega,}, Q^2) + \beta'_{\pi\pi} BW(M_{\omega'}, \Gamma_{\omega'}, Q^2)\right. \\ &\left.\left. + \beta'''_{\pi\pi} BW(M_{\omega''}, \Gamma_{\omega''}, Q^2)\right)\left(\frac{1}{\sqrt{3}}\sin\theta_V \cos\delta - \sin\delta^\omega\right)\sin\delta^\omega\right) \\ &\times \exp\left[\frac{-s}{96\pi^2 F^2}\left(\mathrm{Re}\left[A[m_\pi, M_\rho, Q^2] + \frac{1}{2}A[m_K, M_\rho, Q^2]\right]\right)\right]\,, \end{aligned} \tag{2.13}$$

JHEP03(2021)092

$$
\begin{aligned}
F_V^K = & \left(\frac{\cos\theta_V{}^2}{2}\frac{F_V G_V}{F^2}\left(1+8\sqrt{2}\alpha_V\frac{2m_K^2-m_\pi^2}{M_V^2}\right)M_\phi^2(BW(M_\phi,\Gamma_\phi,Q^2)\right.\\
& \left.+\beta'_{KK}BW(M_{\phi'},\Gamma_{\phi'},Q^2)+\beta''_{KK}BW(M_{\phi''},\Gamma_{\phi''},Q^2)\right)\\
& +\frac{X_1}{24}\frac{F_V G_V}{F^2}\left(1+8\sqrt{2}\alpha_V\frac{m_\pi^2}{M_V^2}\right)M_\omega^2(BW(M_\omega,\Gamma_\omega,Q^2)\\
& +\beta'_{KK}BW(M_{\omega'},\Gamma_{\omega'},Q^2)+\beta''_{KK}BW(M_{\omega''},\Gamma_{\omega''},Q^2))\\
& \times\exp\left[\frac{-q^2}{96\pi^2F^2}\left(\frac{3}{2}\mathrm{Re}(A[m_K,M_\rho,Q^2])\right)\right]\\
& +\frac{X_2}{24}\frac{F_V G_V}{F^2}M_\rho^2\left(1+8\sqrt{2}\alpha_V\frac{m_\pi^2}{M_V^2}\right)(BW(M_\rho,\Gamma_\rho,Q^2)\\
& +\beta'_{KK}BW(M_{\rho'},\Gamma_{\rho'},Q^2)+\beta''_{KK}BW(M_{\rho''},\Gamma_{\rho''},Q^2)\Big)\\
& \times\exp\left[\frac{-q^2}{96\pi^2F^2}\left(\mathrm{Re}\left[A[m_\pi,M_\rho,Q^2]+\frac{1}{2}A[m_K,M_\rho,Q^2]\right]\right)\right]\,. \qquad (2.14)
\end{aligned}
$$

The functions in eqs. (2.13), (2.14) are given by:

$$
\begin{aligned}
\Big[BW(M_V,\Gamma_V,Q^2)\Big]^{-1} &= M_V^2-iM_V\Gamma_V(Q^2)-Q^2\,,\\
A\left(m_P,\mu,Q^2\right) &= \ln\left(m_P^2/\mu^2\right)+\frac{8m_P^2}{Q^2}-\frac{5}{3}+\sigma_P^3\ln\left(\frac{\sigma_P+1}{\sigma_P-1}\right)\,,\\
\sigma_P &\equiv \sqrt{1-4m_P^2/Q^2}\,, \qquad (2.15)
\end{aligned}
$$

and

$$
\begin{aligned}
X_1 &= -16\sqrt{3}\cos\delta\sin\theta_V\sin\delta^\omega(Q^2)-6\cos^2\delta\cos2\theta_V+12\sin^2\delta_\omega(Q^2)+3\cos2\delta+3\,,\\
X_2 &= -6\cos2\theta_V\sin^2\delta^\rho(Q^2)+16\sqrt{3}\cos\delta\sin\theta_V\sin\delta^\rho(Q^2)\\
&\quad +6\sin^2\delta^\rho(Q^2)+6\cos2\delta+6\,, \qquad (2.16)
\end{aligned}
$$

Notice that $X_1 = 12\sin^2\theta_V$ and $X_2 = 12$ in the isospin limit. The angles $\sin\delta^{\rho,\omega}$ related with the $\rho-\omega$ mixing are defined in eq. (2.9). The Q^2 dependence of resonance widths are a debated issue. A thorough proposal within the chiral framework was proposed in ref. [96] for wide resonances. We will use this result for $\Gamma_\rho(Q^2)$, while a parameterization in terms of the on-shell widths, driven by the two-body phase-space decay will be employed for $\Gamma_{\rho',\rho''}(Q^2)$. The precise expressions are collected in ref. [29]. Meanwhile the rest of resonances, that are quite narrow, will be taken constant. Notice that the two-body vector form factors do not include more unknown couplings to those of three-body form factors.

3 Combined fit to experimental data

As we have seen RχT provides a controlled setting to extract information from experimental data. Part of, but not all, of the couplings have been constrained by demanding that Green functions, in this framework, match the asymptotic behaviour of QCD, within the leading

JHEP03(2021)092

term of the OPE expansion, in the high energy limit. The remaining coupling constants, the mixing angles and resonance masses and on-shell widths are left to be determined from the experimental data of cross sections and widths involving vector resonances.

The unknown couplings include $F_V, 2g_4+g_5, d_2, c_3, \alpha_V$, the phenomenological parameters, β'_X and β''_X with $X=\pi,\eta,\pi\pi,KK$, counting for the corresponding strength of the couplings of the V' and V''.[3] The mixing angles of the pseudoscalar singlet and octet θ_P, that of vector singlet and octet θ_V, and the $\rho-\omega$ mixing angle, the energy dependent δ and/or constant δ_0 are also left free. The masses and widths of resonances belonging to heavier second and third multiplets are also fitted around the central values listed in PDG [38].

The last thirty years of experimental work have been very fruitful getting results for the cross-sections we are interested in, as collected in section 1. In order to get results for our parameters we decide to fit the experimental data of cross-sections obtained by dedicated experiments in the last twenty years, i.e. we exclude data older than 2000, with one exception: BESIII [64] measured the cross section of $e^+e^-\to\pi^+\pi^-\pi^0$ with high statistics above 1.05 GeV, while it has a relatively large uncertainty below that energy. Thus we do not fit the data points below 1.05 GeV from this dataset. In addition we also fit the PDG figures [38] for the decay widths of vector resonances whose expressions are collected in appendix A.

Two fits are performed: Fit I uses a uniform energy dependent $\rho-\omega$ mixing according to eq. (2.9). In Fit II, the two body final state cases take into account the energy dependent $\rho-\omega$ mixing, while the other processes are carried out with a constant $\rho-\omega$ mixing angle, see eq. (2.8). The comparison between cross-section data and the fit is shown in figure 1 for the three-pseudoscalar case and figure 2 for the two-pseudocalar case. The captions in the figures collect all data used in the plots and in the fits.

The global fit includes decay widths of related resonances and their results are shown in table 1. The reported errors are obtained, in quadrature, from two components: one arises from the Bootstrap method by varying the central value of experimental data within its error bar, and the other comes from the statistics with dozens of solutions which could also fit to the experimental data sets well. The latter one is the dominant source of error estimation. The cyan bands of all the solutions of Fit II can be found in figure 1 and figure 2. In general, both Fit I and Fit II provide overall reasonable approximations to the experimental figures quoted in the PDG [38].

3.1 Analysis of the results

A comparison between our fitted parameters and those of Fit 4 in ref. [29] is shown in table 2. We also compare the masses and widths of the resonances with those listed in PDG [38]. The fitting procedure is carried out with MINUIT [110].

The quoted errors in the fitted parameters are provided by the Bootstrap method. In general, the parameters in Fit I and Fit II are consistent with those of Fit 4 in ref. [29],

[3] Notice that $X=\pi,\eta$ appear in the three pseudoscalar final state $\pi^+\pi^-\pi^0$ and $\pi^+\pi^-\eta$, respectively and $X=\pi\pi, KK$ denote the two pseudoscalar final state $\pi^+\pi^-$and K^+K^-, respectively.

JHEP03(2021)092

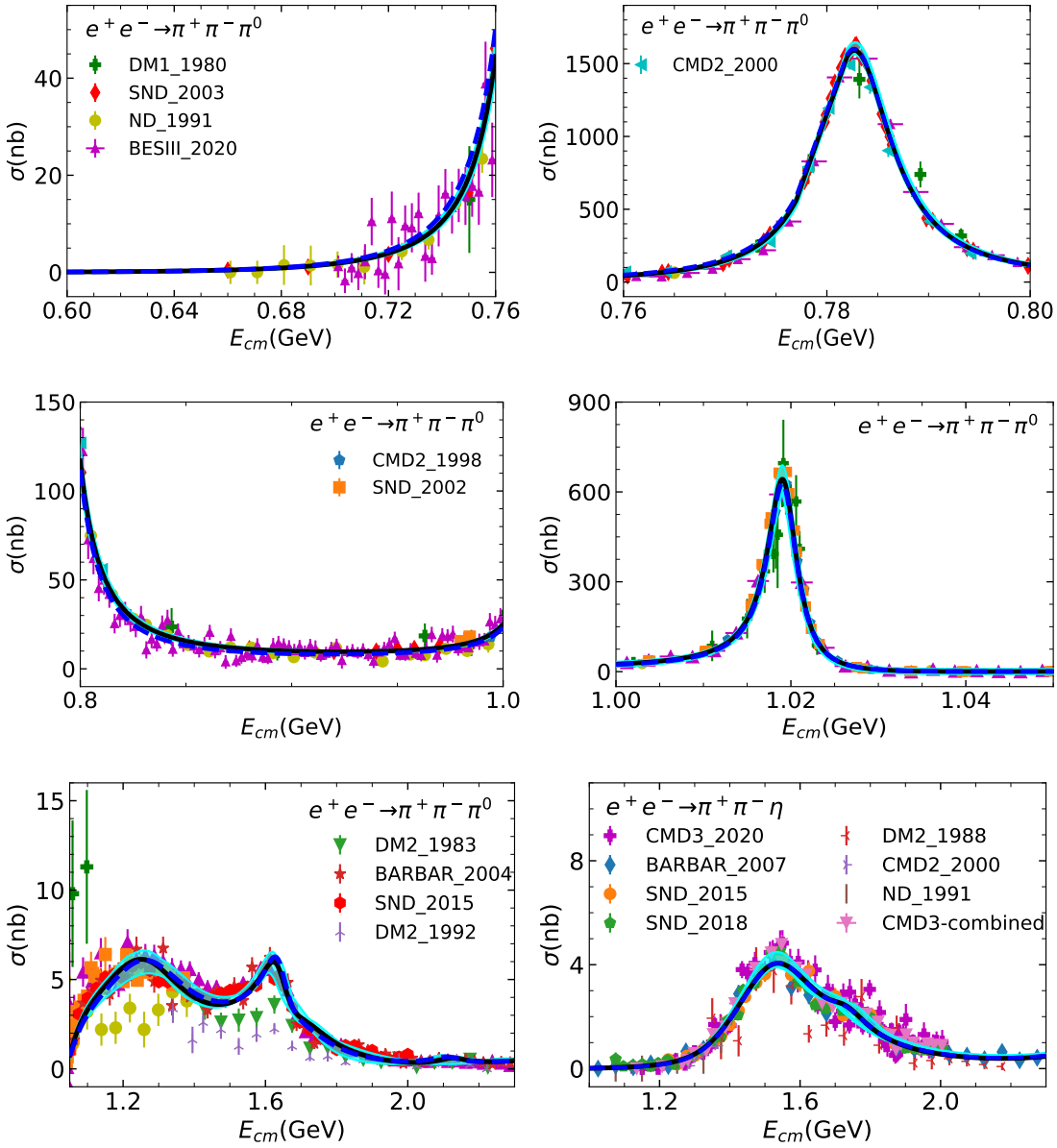

Figure 1. Fit to the cross sections of $e^+e^- \to \pi\pi\pi, \pi\pi\eta$ of Fit I (dashed blue line) and Fit II (solid black line). The cyan bands corresponds to the uncertainty of Fit II. The last graph is about $\eta\pi\pi$ channel and the others for $\pi\pi\pi$. The experimental data displayed for $e^+e^- \to \pi\pi\pi$ are from DM1 [97], ND [98], DM2 [99], CMD2 [100–102], SND [63, 103, 104], Babar [105], and BESIII [64]. The experimental data displayed for $e^+e^- \to \pi\pi\eta$ are from DM2 [106], ND [98], CMD2 [107], Babar [108], SND [65, 66, 109], and CMD3 [67].

within a deviation of about 10%. F_V, $2g_4+g_5$, θ_V, δ_0 and/or δ are mainly determined by the experimental data under 1.05 GeV, where it has higher statistics and precision. However, the joint fit including the $e^+e^- \to K^+K^-$ process constrain θ_V strongly. This can be understood from the form factor in eq. (2.14), where the cross section around the ϕ peak increases with the descent of θ_V. In contrast, the cross section of $e^+e^- \to \pi^+\pi^-\pi^0$ around

JHEP03(2021)092

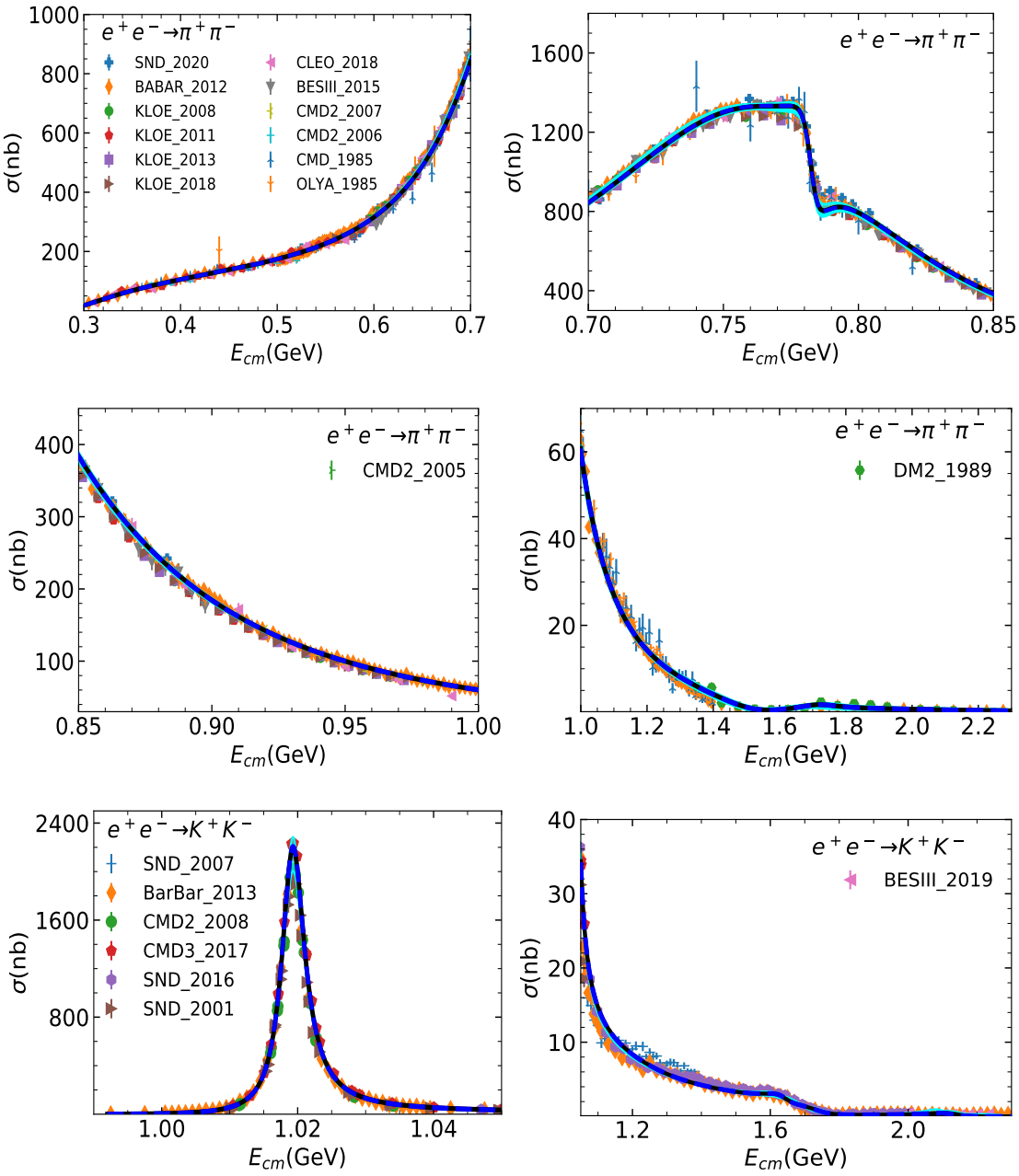

Figure 2. Fit to the cross sections of $e^+e^- \to \pi^+\pi^-, K^+K^-$ of Fit I (dashed blue line) and Fit II (solid black line). The cyan bands correspond to the uncertainty of Fit II. The top four graphs are for $e^+e^- \to \pi^+\pi^-$,the bottom two graphs are for $e^+e^- \to K^+K^-$. The experimental data displayed for $e^+e^- \to \pi^+\pi^-$ are from BaBar [69], KLOE [70–73], SND [74], BESIII [75], CLEO [76], CMD2 [77–79], DM2 [80] and CMD & OLYA [81]. The experimental data displayed for $e^+e^- \to K^+K^-$ are from SND [82–84], BaBar [86], CMD2 [87], CMD3 [88] and BESIII [85].

the ϕ peak decreases when θ_V goes down, which could be deduced from the expressions in appendix A. As a consequence, θ_V is about 1° larger than that of ref. [29]. The inclusion of $e^+e^- \to K^+K^-$ process also constrains α_V, the higher order correction to the F_V coupling

JHEP03(2021)092

arising from SU(3) symmetry breaking. The cross section of $e^+e^- \to K^+K^-$ increases with rising α_V. To confront the theoretical predictions to the experimental data of the cross section of $e^+e^- \to K^+K^-$, α_V is fixed to be negative. Notice that α_V is small as it is higher order correction.

The energy dependent $\rho - \omega$ mixing angle δ is determined by the $e^+e^- \to \pi^+\pi^-$ process. From eq. (2.13), the cross section of $e^+e^- \to \pi^+\pi^-$ is mainly determined by δ, since $F_V G_V/F^2 = 1$ is constrained by the high energy behaviour and θ_V could be determined as above. The two mechanisms of $\rho - \omega$ mixing adopted in Fit I and II have almost no effects on the three body final state case. There is only a very little difference reflected around the ρ peak in the $e^+e^- \to \pi^+\pi^-\pi^0$ process. In the energy region around their masses, ρ and ω mix with a relative phase that results in a larger mode of $|F_V^\pi|^2$. Hence the magnitude of F_V and $2g_4 + g_5$ are smaller in Fit I in comparison to Fit II and the results in ref. [29].

The parameters related with the resonance multiplets are almost the same in Fit I and Fit II, but some of them are different from those of ref. [29]. They are mainly determined by the energy region above 1.0 GeV. Both $e^+e^- \to \pi^+\pi^-$ and $e^+e^- \to \eta\pi^+\pi^-$ processes are sensitive to the masses and widths of $\rho^{'}$ and $\rho^{''}$ in this energy region. The $e^+e^- \to \pi^+\pi^-$ data gives relative smaller masses and larger widths of $\rho^{'}$, compared with those provided by the $e^+e^- \to \eta\pi^+\pi^-$ process. Hence the combined fitted $\rho^{'}$ mass is about 30 MeV smaller and the $\rho^{'}$ width is about 100 MeV larger than those in ref. [29]. The mass and width of $\rho^{''}$ also changes slightly. Consequently, the relative weights of the $e^+e^- \to \eta\pi^+\pi^-$ process β'_η and β''_η have sizable changes compared with those in ref. [29]. Meanwhile, the strengths of the $e^+e^- \to \pi^0\pi^+\pi^-$ process β'_π and β''_π are similar. Notice that in the two-body processes $e^+e^- \to \pi^+\pi^-$ and $e^+e^- \to K^+K^-$, the parameters $\beta_{\pi\pi}^{'('')}$ and $\beta_{KK}^{'('')}$ turn out to be very small with magnitudes $\lesssim 0.2$, as expected by lowest meson dominance [10, 111–114].

Since d_2, c_3 and θ_P are mainly correlated with the $e^+e^- \to \eta\pi^+\pi^-$ process, they also have sizable changes, while masses and widths of other resonance multiplets are quite the same. In summary, and as shown in table 2, the fitted masses and widths of heavier multiplets are closer to the experimental average values in PDG [38], due to a combination of updated experimental measurements and the constraints from $\pi^+\pi^-$ and K^+K^- processes.

Notice however, that the masses and widths of ρ' and ρ'' obtained here correspond to the specific definition of the energy dependent width propagator shown in eq. (40) of ref. [29], which may not be used by the experimentalists. Hence a precise comparison with the experimental determinations is not straightforward.

Finally θ_V and α_V change sizeably with respect to the results of ref. [29] due to the inclusion of the process $e^+e^- \to K^+K^-$, so that the partial widths sensitive to θ_V and α_V become worse. Nevertheless, these partial widths turn out to be bearable with the experimental data from PDG [38], considering the incertitude associated with the theoretical framework of large-N_C expansion implemented in the framework of RχT. In addition, the difference of partial widths of $\Gamma_{\rho^0\to\pi\pi\pi}$ in Fit I and Fit II are caused by the different parametrization of the $\rho - \omega$ mixing. The ρ^0 decays in Fits. I and II have different mixing angles and also the former one is energy dependent, see eq. (2.9).

The comparison of our solutions for the three pseudoscalar case with experimental data is shown in figure 1, and that of the two pseudoscalar case is shown in figure 2. The results

JHEP03(2021)092

Width	Fit 1	Fit II	Ref. [29]	PDG [38]
$\Gamma_{\rho^0\to\pi\pi\pi}$ $(10^{-5}\,\mathrm{GeV})$	0.86±0.31	0.64±0.49	0.93	$1.49^{+0.94}_{-0.73}$
$\Gamma_{\omega\to\pi\pi\pi}$ $(10^{-3}\,\mathrm{GeV})$	7.43±0.78	7.96±0.74	7.66	7.58±0.05
$\Gamma_{\phi\to\pi\pi\pi}$ $(10^{-4}\,\mathrm{GeV})$	9.08±1.57	9.00±1.14	6.25	6.53±0.14
$\Gamma_{\rho\to ee}$ $(10^{-6}\,\mathrm{GeV})$	5.56±0.66	5.81±0.52	6.54	6.98±0.07
$\Gamma_{\omega\to ee}$ $(10^{-7}\,\mathrm{GeV})$	7.28±0.85	7.60±0.65	6.69	6.25±0.13
$\Gamma_{\phi\to ee}$ $(10^{-6}\,\mathrm{GeV})$	0.82±0.09	0.86±0.08	1.20	1.26±0.01
$\Gamma_{\rho\to\pi\pi}$ $(10^{-1}\,\mathrm{GeV})$	1.30±0.17	1.24±0.11	1.14	1.48±0.01
$\Gamma_{\omega\to\pi\pi}$ $(10^{-4}\,\mathrm{GeV})$	1.33±0.47	1.23±0.11	1.61	1.30±0.05
$\Gamma_{\phi\to\pi\pi}$ $(10^{-7}\,\mathrm{GeV})$	1.82±0.20	1.91±0.18	2.66	3.10±0.55
$\Gamma_{\rho^0\to\pi^0\gamma}$ $(10^{-5}\,\mathrm{GeV})$	4.60±0.64	5.38±0.64	5.96	6.95±0.89
$\Gamma_{\rho^+\to\pi^+\gamma}$ $(10^{-5}\,\mathrm{GeV})$	4.46±0.62	4.53±0.37	4.81	6.65±0.74
$\Gamma_{\omega\to\pi^0\gamma}$ $(10^{-4}\,\mathrm{GeV})$	3.97±0.47	4.07±0.35	4.43	7.13±0.19
$\Gamma_{\phi\to\pi^0\gamma}$ $(10^{-6}\,\mathrm{GeV})$	9.01±2.26	9.17±1.30	7.34	5.52±0.21
$\Gamma_{\rho\to\eta\gamma}$ $(10^{-5}\,\mathrm{GeV})$	3.95±0.69	4.32±0.38	4.85	4.43±0.31
$\Gamma_{\omega\to\eta\gamma}$ $(10^{-6}\,\mathrm{GeV})$	4.42±0.77	3.77±0.48	4.13	3.82±0.34
$\Gamma_{\phi\to\eta\gamma}$ $(10^{-5}\,\mathrm{GeV})$	5.92±0.78	6.10±0.48	6.57	5.54±0.11
$\Gamma_{\eta'\to\rho\gamma}$ $(10^{-5}\,\mathrm{GeV})$	4.51±1.34	5.10±1.10	5.37	5.66±0.10
$\Gamma_{\eta'\to\omega\gamma}$ $(10^{-6}\,\mathrm{GeV})$	6.24±1.77	5.52±0.94	5.12	4.74±0.13
$\Gamma_{\phi\to\eta'\gamma}$ $(10^{-7}\,\mathrm{GeV})$	3.07±0.71	3.36±0.44	3.93	2.64±0.09

Table 1. Decay widths involving vector resonances compared with the Fit 4 of ref. [29] and PDG [38].

of Fit I are shown in blue dashed lines and those of Fit II are shown in solid black lines. In general, Fit I and Fit II are almost indistinguishable. There is slight difference shown around the ρ peak in $e^+e^-\to\pi^+\pi^-\pi^0$ process at $0.6 < E < 1$ (GeV), due to the different parametrization of $\rho-\omega$ mixing adopted. Noted that Fit II is a little better in this region, since there is one more parameter δ_0 and the energy dependent mixing mechanism designed for the $\pi\pi$ scattering may not be suitable for the three pion case, where the three body re-scattering needs to be considered. Fit II seems also a little better at the ϕ peak in the $e^+e^-\to\pi^+\pi^-\pi^0$ process. This is because that, F_V and $2g_4+g_5$ in Fit II are allowed to have larger values than in Fit I, which can slightly compensate the ϕ peak in $e^+e^-\to\pi^+\pi^-\pi^0$. As illustrated above, the θ_V and α_V constrained by the $e^+e^-\to K^+K^-$ will suppress the ϕ peak in $e^+e^-\to\pi^+\pi^-\pi^0$. The high energy behaviour of $e^+e^-\to\pi^+\pi^-$, as shown in figure 2, is balanced with the $e^+e^-\to\eta\pi^+\pi^-$ process through the mass and width of $\rho^{'}$.

4 Leading-order hadronic vacuum polarization contributions to a_μ

The Hadronic Vacuum Polarization (HVP) corrections to $a_\mu = (g_\mu - 2)/2$ are related to the $e^+e^-\to$ hadrons cross sections through the optical theorem and analyticity [40, 115].

JHEP03(2021)092

	Fit I	Fit II	Ref. [29]	PDG [38]
F_V (GeV)	0.139±0.001	0.142±0.001	0.148±0.001	—
$2g_4 + g_5$	−0.442±0.001	−0.492±0.002	−0.493±0.003	—
d_2	0.0273±0.0005	0.0276±0.0006	0.0359±0.0007	—
c_3	0.00432±0.00012	0.00435±0.00013	0.00689±0.00017	—
α_V	−0.00120±0.00012	−0.00113±0.00014	0.0126±0.0007	—
$\theta_V(^\circ)$	39.61±0.01	39.56±0.01	38.94±0.02	—
$\theta_P(^\circ)$	-19.39±0.09	-19.61±0.10	-21.37±0.26	—
$\delta_0(^\circ)$	—	1.70±0.05	2.12±0.06	—
$\delta(^\circ)$	-1.83±0.04	-1.80±0.01	—	—
β'_π	−0.434±0.005	−0.454±0.003	−0.469±0.008	—
β''_π	0.239±0.002	0.224±0.005	0.225±0.007	—
β'_η	−0.452±0.008	−0.438±0.006	−0.174±0.017	—
β''_η	−0.0213±0.0031	−0.0233±0.0023	−0.0968±0.0139	—
$\beta'_{\pi\pi}$	−0.0625±0.0007	−0.0625±0.0009	—	—
$\beta''_{\pi\pi}$	0.0115±0.0006	0.0118±0.0007	—	—
β'_{KK}	−0.0652±0.0023	−0.0712±0.0040	—	—
β''_{KK}	−0.202±0.003	−0.197±0.005	—	—
$M_{\rho'}$ (GeV)	1.517±0.001	1.519±0.002	1.550±0.012	1.465(25)
$\Gamma_{\rho'}$ (GeV)	0.340±0.006	0.340±0.001	0.238±0.018	0.400(60)
$M_{\omega'}$ (GeV)	1.256±0.006	1.253±0.003	1.249±0.003	1.410(60)
$\Gamma_{\omega'}$ (GeV)	0.310±0.005	0.310±0.003	0.307±0.007	0.290(190)
$M_{\phi'}$ (GeV)	1.640±0.003	1.640±0.003	1.641±0.005	1.680(20)
$\Gamma_{\phi'}$ (GeV)	0.083±0.001	0.090±0.002	0.086±0.007	0.15(5)
$M_{\rho''}$ (GeV)	1.720±0.004	1.720±0.001	1.794±0.012	1.720(20)
$\Gamma_{\rho''}$ (GeV)	0.150±0.001	0.150±0.005	0.297±0.033	0.25(10)
$M_{\omega''}$ (GeV)	1.683±0.005	1.725±0.010	1.700±0.011	1.670(30)
$\Gamma_{\omega''}$ (GeV)	0.400±0.002	0.400±0.003	0.400±0.013	0.315(35)
$M_{\phi''}$ (GeV)	2.114±0.010	2.126±0.025	2.086±0.022	2.160(80)
$\Gamma_{\phi''}$ (GeV)	0.108±0.014	0.100±0.014	0.108±0.017	0.125(65)

Table 2. Fitted parameters of Fits I and II compared with the Fit 4 of ref. [29] and PDG [38]. The uncertainty of the parameters are coming from the Bootstrap method.

JHEP03(2021)092

The leading order HVP correction can be expressed as

$$a_\mu^{\rm had} = \left(\frac{\alpha_e(0) m_\mu}{3\pi}\right)^2 \int_{s_{\rm thr}}^{\infty} {\rm d}s \frac{\hat{K}(s)}{s^2} R_{\rm h}(s)\,, \tag{4.1}$$

where

$$\alpha_e = \frac{e^2}{4\pi}, \qquad R_{\rm h}(s) = \frac{3s}{4\pi\alpha_e^2(s)}\,\sigma\left(e^+e^- \to \text{ hadrons }\right)\,, \tag{4.2}$$

and the kernel function is defined as,

$$\hat{K}(s) = \frac{3s}{m_\mu^2}\left[\frac{(1+x^2)\,(1+x)^2}{x^2}\left(\ln(1+x) - x + \frac{x^2}{2}\right) + \frac{x^2}{2}\left(2-x^2\right) + \frac{1+x}{1-x}x^2\ln x\right]\,, \tag{4.3}$$

with

$$x = \frac{1-\beta_\mu(s)}{1+\beta_\mu(s)}, \qquad \beta_\mu(s) = \sqrt{1-\frac{4m_\mu^2}{s}}\,. \tag{4.4}$$

Notice that the lower limit in the integration in eq. (4.1) depends on the starting contribution and its $\mathcal{O}(\alpha_e)$ order. Hence $s_{\rm thr} = m_{\pi^0}^2$ when including the $\pi^0\gamma$ contribution and $s_{\rm thr} = 4m_\pi^2$ when starting in the $\pi\pi$ contribution.

It is interesting to notice the $1/s^2$ enhancement factor (leading order) of contributions of low energies in $a_\mu^{\rm had}$ (3). Thus the kernel gives higher weight, in particular, to the lowest lying resonance $\rho(770)$ that couples strongly to $\pi^+\pi^-$. This fact is the reason why the pion pair production $e^+e^- \to \pi^+\pi^-$ gives, by far, the largest contribution to $a_\mu^{\rm had}$. However, we are in the position to determine the contributions to the muon anomalous magnetic moment relevant to the three and two pseudoscalar final states that we discussed above. They are shown as a_μ^C with different energy regions in table 3.

Here a_μ^C $(C = \pi\pi, KK, \pi\pi\pi, \eta\pi\pi)$ denotes for the lowest order hadronic vacuum polarization contribution of $e^+e^- \to \pi\pi, KK, \pi\pi\pi, \eta\pi\pi$, respectively. The error bars for a_μ^C are given by the combination of the uncertainty coming from the Bootstrap method and the statistics from dozens of solutions that also fit to the experimental data sets well.

It is noted that, although different parameterizations of the $\rho-\omega$ mixing are adopted in Fit I and Fit II, the individual contributions of each channel are almost the same. A look back to the figure 1 shows that the results of Fit I are slightly different from the ones of Fit II around the ρ peak in the $e^+e^- \to \pi^+\pi^-\pi^0$ process (see the first three graphs). However, the total contributions to $a_\mu^{\pi\pi\pi}|_{\le 1.8\,{\rm GeV}}$ are almost the same, as the contribution of Fit I is slightly larger than that of Fit II on the left hand side of he ρ peak, but it is in the opposite situation on the right hand side of ρ peak. They tend to cancel between each other. Since there is little difference between the two fits, we will discuss below with Fit II. The a_μ^C evaluated here are consistent with those in refs. [60, 116, 117], within their uncertainty. In addition, $a_\mu^{\pi\pi\pi}|_{\le 1.8\,{\rm GeV}}$ is also consistent with that evaluated based on the cross section fitted in ref. [29]. On the other hand, a slightly larger $a_\mu^{\eta\pi\pi}|_{\le 1.8\,{\rm GeV}}$ is obtained compared with that of refs. [29, 60]. One has to note that the $e^+e^- \to \eta\pi^+\pi^-$ process

JHEP03(2021)092

$a_\mu^C \times 10^{-10}$	Ref. [116]	Ref. [29]	Ref. [117]	Ref. [60]	Fit I	Fit II
$a_\mu^{\pi\pi}\|_{\leq 0.63\text{GeV}}$	132.8(0.4)(1.0)	—	—	—	132.11±0.63	132.11±0.67
$a_\mu^{\pi\pi}\|_{\leq 1\text{GeV}}$	495.0(1.5)(2.1)	—	—	—	498.48±2.34	498.47±2.33
$a_\mu^{\pi\pi}\|_{\leq 1.8\text{GeV}}$	—	—	—	507.85±0.83±3.23±0.55	508.89±2.45	508.89±2.45
$a_\mu^{\pi\pi}\|_{\leq 2.3\text{GeV}}$	—	—	—	—	509.13±2.48	509.13±2.48
$a_\mu^{KK}\|_{\leq .1.1\text{GeV}}$	—	—	—	—	20.73±0.94	20.74±0.88
$a_\mu^{KK}\|_{\leq .1.8\text{GeV}}$	—	—	—	23.08±0.20±0.33±0.21	24.35±1.02	24.36±0.97
$a_\mu^{KK}\|_{\leq 2.3\text{GeV}}$	—	—	—	—	24.43±1.03	24.44±1.01
$a_\mu^{\pi\pi\pi}\|_{\leq 1.8\text{GeV}}$	—	48.55	46.2(8)	46.21±0.40±1.10±0.86	48.55±1.42	48.54±1.39
$a_\mu^{\pi\pi\pi}\|_{\leq 2.3GeV}$	—	—	—	—	48.76±1.45	48.75±1.43
$a_\mu^{\eta\pi\pi}\|_{\leq 1.8\text{GeV}}$		1.135	—	1.19±0.02±0.04±0.02	1.28±0.10	1.29±0.09
$a_\mu^{\eta\pi\pi}\|_{\leq 2.3GeV}$	—	—	—	—	1.52±0.12	1.53±0.12
$a_\mu^{\text{HVP.LO}}$	—	—	—	694.0±4.0	699.46±3.41	699.47±3.39
a_μ^{SM}				11659183.1±4.8	11659187.3±3.8	11659187.3±3.9
Δa_μ				$26.0 \pm 7.9(3.3\sigma)$	$21.6 \pm 7.4(2.9\sigma)$	$21.6 \pm 7.4(2.9\sigma)$

Table 3. Our predictions of muon anomalous magnetic moment, where other contributions are from refs. [39, 60] and references therein. We compared the a_μ^C , $a_\mu^{\text{HVP,LO}}$, a_μ^{SM} and Δa_μ with refs. [29, 60, 116, 117]. The experimental value is measured as $a_\mu^{\text{exp}} = 11659208.9 \pm 6.3$ [37].

has a threshold at about 0.73 GeV, and therefore has a larger dependence on the resonance multiplets.

As explained above the largest contribution of the hadronic vacuum polarization comes from $e^+e^- \to \pi^+\pi^-$. In our theoretical framework, the cross section of $e^+e^- \to \pi^+\pi^-$ below 1 GeV is almost fixed with a small dependence on δ, while other parameters contribute little. Hence the $e^+e^- \to \pi^+\pi^-$ cross-section shares little uncertainty from the parameters. For the $e^+e^- \to K^+K^-$ process, only θ_V and α_V are sensitive, but θ_V and α_V are in tension with the ϕ peak in $e^+e^- \to \pi^+\pi^-\pi^0$. Hence, there is a dedicated balance between these two data sets, which causes considerable uncertainty. Since we have fitted up to $E = 2.3\,\text{GeV}$, we also listed the corresponding $a_\mu^C|_{\leq 2.3\,\text{GeV}}$ in table 3.

The total contribution is

$$a_\mu^{\text{HVP,LO}} = (699.47 \pm 3.38) \times 10^{-10} \tag{4.5}$$

from Fit II, in combination with the left channels fitted in ref. [60]. Note that the four contributions we consider here provide the largest uncertainty among all the channels. Combined with the other contributions (QED [41], EW [43–46], NLHVP [62], NNLHVP [62], HLBL [39, 47–49]) within the SM, we also give an estimation of the anomalous magnetic moment of muon in SM. It is about 4.2×10^{-10} larger in total than that in ref. [60]. Hence our estimation of the discrepancy Δa_μ between the theoretical prediction in SM and that measured by experiment is 0.4σ smaller than that in ref. [60]. Our estimation of $\Delta a_\mu = (21.6 \pm 7.4) \times 10^{-10}$ is 2.9σ smaller than that of the experimental value.

JHEP03(2021)092

5 Higher-order hadronic vacuum polarization contributions to a_μ

We can also consider the contribution of the hadronic vacuum polarization to higher-order corrections to the leading result of the previous section 4. These have already been computed in the past at next-to-leading (NLO) order [118] and nex-to-next-to-leading (NNLO) order [62]. In our case, however, we will only consider the contribution of two and three pseudoscalars to HVP, as we have obtained in section 3.

NLO contributions correspond to $\mathcal{O}(\alpha_e^3)$ with one and two HVP insertions. They are given by

$$\begin{aligned} a_\mu^{(2a,2b)} &= \frac{1}{3}\left(\frac{\alpha_e(0)}{\pi}\right)^3 \int_{4m_\pi^2}^\infty \frac{ds}{s}\, R_{\rm h}(s)\; K^{(2a,2b)}(s)\,, \\ a_\mu^{(2c)} &= \frac{1}{9}\left(\frac{\alpha_e(0)}{\pi}\right)^3 \iint_{4m_\pi^2}^\infty \frac{ds}{s}\frac{ds'}{s'} R_{\rm h}(s)\, R_{\rm h}\left(s'\right)\; K^{(2c)}\left(s,s'\right)\,, \end{aligned} \tag{5.1}$$

respectively, where $R_{\rm h}(s)$ has been defined in eq. (4.2). The label notation and the kernels $K^{(2a,2b,2c)}$ can be read from ref. [118]. Notice that the lower limit in the integral is taken to be $4m_\pi^2$ as we are only including the contribution of cross-sections of two and three pseudoscalars.

$\mathcal{O}(\alpha_e^4)$ with up to three HVP insertions corresponds to the NNLO case. Their contributions can be computed as

$$\begin{aligned} a_\mu^{(3a,3b,3bLBL)} &= \frac{1}{3}\left(\frac{\alpha_e(0)}{\pi}\right)^4 \int_{4m_\pi^2}^\infty \frac{ds}{s}\, R_{\rm h}(s)\, K^{(3a,3b,3bLBL)}(s)\,, \\ a_\mu^{(3c)} &= \frac{1}{9}\left(\frac{\alpha_e(0)}{\pi}\right)^4 \iint_{4m_\pi^2}^\infty \frac{ds}{s}\frac{ds'}{s'} R_{\rm h}(s)\, R_{\rm h}\left(s'\right)\; K^{(3c)}\left(s,s'\right)\,, \\ a_\mu^{(3d)} &= \frac{1}{27}\left(\frac{\alpha_e(0)}{\pi}\right)^4 \iiint_{4m_\pi^2}^\infty \frac{ds}{s}\frac{ds'}{s'}\frac{ds''}{s''} R_{\rm h}(s)\, R_{\rm h}\left(s'\right)\, R_{\rm h}\left(s''\right)\; K^{(3d)}\left(s,s',s''\right)\,. \end{aligned} \tag{5.2}$$

Here the label notation and the different kernels $K^{(3a,3b,3bLBL,3c,3d)}$ follow from ref. [62].

Our results are shown in table 4. Since Fit I and Fit II are almost indistinguishable, we would just derive the higher order HVP corrections with Fit II. We also quote the results of ref. [62], although we remind that the later include all the cross sections but not only the two- and three-pseudoscalar contributions (with $\sqrt{s} \leq 2.3\,\text{GeV}$) to HVP that we have computed. Hence, the difference between both results can be considered as an estimate of the HVP contributions, that we have not included, and of the higher-energy contribution of the two- and three-pseudoscalar channels. The errors have been estimated in the same way as the leading order contributions to a_μ^C. It is found that these four processes (with the quoted energy upper limit) account for roughly 70 percent of the higher-order HVP corrections to $a_\mu^{\rm had}$.

6 Conclusions

Combined with the latest experimental data available for e^+e^- annihilation into three pseudoscalar cases $e^+e^- \to \pi\pi\pi, \pi\pi\eta$, we carried out joint fits including the two pseudoscalar

JHEP03(2021)092

$\times 10^{-12}$	$\pi\pi$	KK	$\pi\pi\pi$	$\pi\pi\eta$	Our total	Total [62]
2a	−1369±8	−79.8±2.8	−145±3	−5.93±0.46	−1600±9	−2090
2b	776±5	37.6±1.3	74.7±1.8	2.37±0.18	891±5	1068
2c			22.4±0.2		22.4±0.2	35
$a_\mu^{\rm NLO}$					−687±10	−987±9
3a	45.4±0.3	3.11±0.11	5.20±0.12	0.267±0.021	54.0±0.3	80
3b	−24.8±0.2	−1.62±0.06	−2.78±0.06	−0.131±0.010	−29.3±0.2	−41
3bLBL	58.0±0.3	3.47±0.12	6.19±0.14	0.268±0.021	67.9±0.4	91
3c			−2.34±0.02		−2.34±0.02	−6
3d			0.0249±0.0004		0.0249±0.0004	0.05
$a_\mu^{\rm NNLO}$					90.3±0.5	124±1

Table 4. Our estimation of the higher-order HVP contributions to $a_\mu^{\rm had}$ using Fit II results and with and upper limit of integration of $\sqrt{s} = 2.3\,\text{GeV}$. The sum of the four processes considered here is given in the penultimate column, while the contributions of all channels, estimated in ref. [62], are listed in the last column.

cases $e^+e^- \to \pi^+\pi^-, K^+K^-$, within the framework of RχT in the energy region up to $E \lesssim 2\,\text{GeV}$. Taking into account the possible different mixing mechanisms of $\rho - \omega$ in the three and two pseudoscalar cases, two fits have been performed. In Fit I, we apply a uniform energy dependent $\rho - \omega$ mixing parametrization. In Fit II, the energy dependent $\rho - \omega$ mixing parametrization is only used in the two pseudoscalar channel, while a constant mixing angle is used in the three body case. Overall very reasonable fits for both cases are found. There is no relevant difference between Fit I and Fit II except for a small difference around the ρ peak in the $\pi^+\pi^-\pi^0$ case. This indicates that the $\rho - \omega$ mixing mechanism that plays an important role in the two pion case may not be exactly the one to be applied in the three body case. However, it will not affect much the descriptions in the three body case, as well as their contribution to the HVP. Our results have been obtained within a QCD-based phenomenological theory framework with a joint fit of four different channels that restrict mutually each other.

The main hadronic contributions to the muon anomalous magnetic moment come from the lower energy region $E < 1.05\,\text{GeV}$ of the hadronic vacuum polarization input, where few parameters are dominant. Hence, reliable predictions can be made within our theoretical framework from our previous analyses of the two- and three-pseudoscalar contributions to the e^+e^- cross-section. Accordingly we have computed the leading-order HVP contribution to the anomalous magnetic moment of the muon by including the four main channels, studied previously, in our estimate. The central value of these four channels to HVP is about 5×10^{-10} larger than that of ref. [60]. In consequence, the discrepancy between SM prediction and the experimental measurement decreases to $(21.6 \pm 7.4) \times 10^{-10}$. As an aside, we have also computed the NLO and NNLO HVP contributions to the anomalous magnetic moment of the muon as given by the two- and three-pseudoscalar contributions to the cross-section.

JHEP03(2021)092

Acknowledgments

We thank for the useful discussions with professors Chu-Wen Xiao and Jian-Ming Shen. This project is supported by National Natural Science Foundation of China (NSFC) with Grant Nos. 11805059 and 11675051, Joint Large Scale Scientific Facility Funds of the NSFC and Chinese Academy of Sciences (CAS) under Contract No. U1932110, and Fundamental Research Funds for the Central Universities. This work has been supported in part by Grants No. FPA2017-84445-P and SEV-2014-0398 (AEI/ERDF, EU) and by PROMETEO/2017/053 (GV).

A Three body final state form factors and partial decay widths

A.1 Three body final state form factor

The cross section of the $e^+e^- \to \pi^+(p_1)\pi^-(p_2)P(p_3)$ process (P a pseudoscalar meson) is driven by the vector form factor in eq. (2.10) through

$$\sigma_P(Q^2) = \frac{\alpha^2}{192\,\pi\,Q^6}\int_{s_-}^{s_+} ds \int_{t_-}^{t_+} dt\,\phi(Q^2,s,t)\,|F_V^P(Q^2,s,t)|^2, \tag{A.1}$$

where $Q = p_1+p_2+p_3$, $s=(Q-p_3)^2$, $t=(Q-p_1)^2$ and

$$\begin{aligned}\phi(Q^2,s,t) =& st(Q^2-s-t) + sm_P^2(t-Q^2)\\ &- m_\pi^2[m_P^4 - m_P^2(2Q^2+s) + Q^4 - Q^2 s - 2st] - sm_\pi^4\,,\end{aligned} \tag{A.2}$$

being $m_P = m_\pi, m_\eta$, depending on the final state. In eq. (A.1) the integration limits are:

$$\begin{aligned} s_- &= 4m_\pi^2\,,\\ s_+ &= \left(\sqrt{Q^2}-m_P\right)^2,\\ t_\pm &= \frac{1}{4\,s}\left\{\left(Q^2-m_P^2\right)^2 - \left[\lambda^{1/2}(Q^2,s,m_P^2) \mp \lambda^{1/2}(s,m_\pi^2,m_\pi^2)\right]^2\right\}, \end{aligned} \tag{A.3}$$

with $\lambda(a,b,c)$ the Källén's triangle function.

The vector form factors relevant for the $e^+e^- \to \pi^+\pi^-\pi^0$, $\pi^+\pi^-\eta$ cross-sections are given by:

$$F_V^P(Q^2,s,t) = F_a^P + F_b^P + F_c^P + F_d^P\,, \tag{A.4}$$

with $P=\pi,\eta$. We give now the expressions for the form factors. When notation is not fully specified we refer to appendix A.3 of ref. [29].

Hence the vector form factors are

$$F_a^\pi = -\frac{N_C}{12\pi^2 F^3},$$

$$F_b^\pi = \frac{8\sqrt{2}F_V(1+8\sqrt{2}\alpha_V\frac{m_\pi^2}{M_V^2})}{3M_V F^3}(\sqrt{2}\cos\theta_V + \sin\theta_V)\,G_{R_\pi}(Q^2)$$

JHEP03(2021)092

$$
\begin{aligned}
&\times \Big\{(\sin\theta_V\cos\delta-\sqrt{3}\sin\delta^{\omega}(Q^2))\cos\delta BW_R[\pi,\omega,Q^2]\\
&+(\sin\theta_V\sin\delta^{\rho}(Q^2)+\sqrt{3}\cos\delta)\sin\delta^{\rho}(Q^2)\ BW_R[\pi,\rho,Q^2]\Big\}\\
&+\frac{8\sqrt{2}F_V(1+8\sqrt{2}\alpha_V\frac{2m_K^2-m_\pi^2}{M_V^2})}{3M_VF^3}\cos\theta_V(\cos\theta_V-\sqrt{2}\sin\theta_V)\,BW_R[\pi,\phi,Q^2]\ G_{R_\pi}(Q^2),\\
F_c^{\pi}=&-\frac{4\sqrt{2}G_V}{3M_VF^3}\Big\{(\cos\delta+\sqrt{6}\cos\theta_V\sin\delta^{\rho}(s)+\sqrt{3}\sin\delta^{\rho}(s)\sin\theta_V)\cos\delta\\
&\times BW_R[\pi,\rho,s]\ C_{R\pi}(Q^2,s)+BW_R[\pi,\rho,t]\ C_{R\pi}(Q^2,t)+BW_R[\pi,\rho,u]\ C_{R\pi}(Q^2,u)\\
&-\Big[\sqrt{3}\cos\delta\left(\sqrt{2}\cos\theta_V+\sin\theta_V\right)-\sin\delta^{\omega}(s)\Big]\sin\delta^{\omega}(s)\ BW_R[\pi,\omega,s]\ C_{R\pi}(Q^2,s)\Big\},\\
F_d^{\pi}=&\frac{8G_VF_V(1+8\sqrt{2}\alpha_V\frac{{m_\pi}^2}{M_V^2})}{3F^3}(\sqrt{2}\cos\theta_V+\sin\theta_V)\\
&\times\Big\{(\sin\theta_V\cos\delta-\sqrt{3}\sin\delta^{\omega}(Q^2))\cos\delta(\cos^2\delta-\sin\delta^{\rho}(s)\sin\delta^{\omega}(Q^2))\\
&\times BW_{RR}[\pi,\omega,\rho,Q^2,s]D_{R\pi}(Q^2,s)\\
&+(\sin\theta_V\cos\delta-\sqrt{3}\sin\delta^{\omega}(Q^2))\cos\delta\ BW_{RR}[\pi,\omega,\rho,Q^2,t]\ D_{R\pi}(Q^2,t)\\
&+(\sin\theta_V\cos\delta-\sqrt{3}\sin\delta^{\omega}(Q^2))\cos\delta\ BW_{RR}[\pi,\omega,\rho,Q^2,u]\ D_{R\pi}(Q^2,u)\\
&+(\sin\theta_V\cos\delta-\sqrt{3}\sin\delta^{\omega}(Q^2))[\sin\delta^{\omega}(Q^2)+\sin\delta^{\omega}(s)]\cos\delta\sin\delta^{\omega}(s)\\
&\times BW_{RR}[\pi,\omega,\omega,Q^2,s]D_{R\pi}(Q^2,s)\\
&+(\sin\theta_V\sin\delta^{\rho}(Q^2)+\sqrt{3}\cos\delta)[\sin\delta^{\rho}(Q^2)+\sin\delta^{\rho}(s)]\cos^2\delta\\
&\times\ BW_{RR}[\pi,\rho,\rho,Q^2,s]\ D_{R\pi}(Q^2,s)\\
&+(\sin\theta_V\sin\delta^{\rho}(Q^2)+\sqrt{3}\cos\delta)\sin\delta^{\rho}(Q^2)\ BW_{RR}[\pi,\rho,\rho,Q^2,t]\ D_{R\pi}(Q^2,t)\\
&+(\sin\theta_V\sin\delta^{\rho}(Q^2)+\sqrt{3}\cos\delta)\sin\delta^{\rho}(Q^2)\ BW_{RR}[\pi,\rho,\rho,Q^2,u]\ D_{R\pi}(Q^2,u)\\
&-(\sin\theta_V\sin\delta^{\rho}(Q^2)+\sqrt{3}\cos\delta)(\cos^2\delta-\sin\delta^{\rho}(Q^2)\sin\delta^{\omega}(s))\sin\delta^{\omega}(s)\\
&\times BW_{RR}[\pi,\rho,\omega,Q^2,s]D_{R\pi}(Q^2,s)\Big\}\\
&+\frac{8G_VF_V(1+8\sqrt{2}\alpha_V\frac{2{m_K}^2-{m_\pi}^2}{M_V^2})}{3F^3}(\cos\theta_V-\sqrt{2}\sin\theta_V)\ \cos\theta_V\\
&\times\Big\{\cos^2\delta BW_{RR}[\pi,\phi,\rho,Q^2,s]D_{R\pi}(Q^2,s)+\sin^2\delta^{\omega}(s)BW_{RR}[\pi,\phi,\omega,Q^2,s]D_{R\pi}(Q^2,s)\\
&+BW_{RR}[\pi,\phi,\rho,Q^2,t]\ D_{R\pi}(Q^2,t)+\ BW_{RR}[\pi,\phi,\rho,Q^2,u]\ D_{R\pi}(Q^2,u)\Big\}\ ,\\
F_a^{\eta}=&-\frac{N_C}{12\sqrt{3}\pi^2F^3}(-\sqrt{2}\sin\theta_P+\cos\theta_P),\\
F_b^{\eta}=&\frac{8\sqrt{6}F_V(1+8\sqrt{2}\alpha_V\frac{m_\pi^2}{M_V^2})}{3M_VF^3}\left(\cos\delta+\frac{1}{\sqrt{3}}\sin\delta^{\rho}(Q^2)\sin\theta_V\right)\\
&\times\cos\delta(-\sqrt{2}\sin\theta_P+\cos\theta_P)BW_R[\eta,\rho,Q^2]\ G_{R\eta}(Q^2,s)\\
&-\frac{8\sqrt{6}F_V(1+8\sqrt{2}\alpha_V\frac{m_\pi^2}{M_V^2})}{3M_VF^3}\left(-\sin\delta^{\omega}(Q^2)+\frac{1}{\sqrt{3}}\cos\delta\sin\theta_V\right)\sin\delta^{\omega}(Q^2)\\
&\times(-\sqrt{2}\sin\theta_P+\cos\theta_P)BW_R[\eta,\omega,Q^2]\ G_{R\eta}(Q^2,s),
\end{aligned}
$$

$$
\begin{aligned}
F_c^{\eta} = & -\frac{4\sqrt{2}G_V}{3M_V F^3}\cos\delta\Big\{\sqrt{3}\cos\delta(\cos\theta_P-\sqrt{2}\sin\theta_P)+\sin\delta^{\rho}(s)\ [\ \sqrt{2}\cos\theta_V\cos\theta_P \\
& -\sin\theta_V(\cos\theta_P+\sqrt{2}\sin\theta_P)]\Big\}BW_R[\eta,\rho,s]\ C_{R\eta 1}(Q^2,s,m_\eta^2) \\
& -\frac{4\sqrt{2}G_V}{9M_V F^3}\cos\delta\{4\sin\delta^{\rho}(s)[\sqrt{2}\cos(\theta_V+\theta_P)-2\cos\theta_P\sin\theta_V+\cos\theta_V\sin\theta_P]m_K^2 \\
& +[3\sqrt{3}\cos\delta(\cos\theta_P-\sqrt{2}\sin\theta_P)-\sin\delta^{\rho}(s)(\sqrt{2}\cos(\theta_V+\theta_P)-5\cos\theta_P\sin\theta_V \\
& +4\cos\theta_V\sin\theta_P\ )]m_\pi^2\}\ BW_R[\eta,\rho,s]\ C_{R\eta 2} \\
& +\frac{4\sqrt{2}G_V}{3M_V F^3}\sin\delta^{\omega}(s)\Big\{\sqrt{3}\sin\delta^{\omega}(s)(-\cos\theta_P+\sqrt{2}\sin\theta_P)+\cos\delta[\sqrt{2}\cos\theta_V\cos\theta_P \\
& -\sin\theta_V(\cos\theta_P+\sqrt{2}\sin\theta_P)]\Big\}\ BW_R[\eta,\omega,s]\ C_{R\eta 1}(Q^2,s,m_\eta^2) \\
& +\frac{4\sqrt{2}G_V}{9M_V F^3}\sin\delta^{\omega}(s)\Big\{4\cos\delta[\sqrt{2}\cos(\theta_V+\theta_P)-2\cos\theta_P\sin\theta_V+\cos\theta_V\sin\theta_P]m_K^2 \\
& -[3\sqrt{3}\sin\delta^{\omega}(s)(\cos\theta_P-\sqrt{2}\sin\theta_P)+\cos\delta(\sqrt{2}\cos(\theta_V+\theta_P)-5\cos\theta_P\sin\theta_V \\
& +4\cos\theta_V\sin\theta_P)]m_\pi^2\Big\}\ BW_R[\eta,\omega,s]\ C_{R\eta 2}, \\
F_d^{\eta} = & \frac{8F_V(1+8\sqrt{2}\alpha_V\frac{m_\pi^2}{M_V^2})G_V}{\sqrt{6}F^3}\cos\delta\left(\cos\delta+\frac{1}{\sqrt{3}}\sin\delta^{\rho}(Q^2)\sin\theta_V\right) \\
& \times\Big\{\cos^2\delta(\sqrt{2}\cos\theta_P-2\sin\theta_P)+\sin\delta^{\rho}(Q^2)\sin\delta^{\rho}(s)[\cos\theta_P\sin\theta_V(4\cos\theta_V \\
& -\sqrt{2}\sin\theta_V)-2\sin\theta_P]\Big\}BW_{RR}[\eta,\rho,\rho,Q^2,s]\ D_{R\eta 1}(Q^2,s,m_\eta^2) \\
& +\frac{2F_V(1+8\sqrt{2}\alpha_V\frac{m_\pi^2}{M_V^2})G_V}{3\sqrt{6}F^3}\cos\delta\left(\cos\delta+\frac{1}{\sqrt{3}}\sin\delta^{\rho}(Q^2)\sin\theta_V\right) \\
& \times\Big\{8\sin\delta^{\rho}(Q^2)\sin\delta^{\rho}(s)[\cos\theta_P(-3\sqrt{2}+\sqrt{2}\cos 2\theta_V+4\sin 2\theta_V) \\
& +(-3+\cos 2\theta_V+2\sqrt{2}\sin 2\theta_V)\sin\theta_P]m_K^2+[12\cos^2\delta(\sqrt{2}\cos\theta_P-2\sin\theta_P) \\
& +\sin\delta^{\rho}(Q^2)\sin\delta^{\rho}(s)(-9\sqrt{2}\cos(2\theta_V-\theta_P)+18\sqrt{2}\cos\theta_P \\
& +7\sqrt{2}\cos(2\theta_V+\theta_P)-8\sin(2\theta_V+\theta_P))]m_\pi^2\Big\}BW_{RR}[\eta,\rho,\rho,Q^2,s]D_{R\eta 2} \\
& -\frac{8F_V(1+8\sqrt{2}\alpha_V\frac{m_\pi^2}{M_V^2})G_V}{\sqrt{6}F^3}\sin\delta^{\omega}(s)\left(-\sin\delta^{\omega}(Q^2)+\frac{1}{\sqrt{3}}\cos\delta\sin\theta_V\right) \\
& \times\Big\{\cos\theta_P[\sqrt{2}\sin\delta^{\omega}(Q^2)\sin\delta^{\omega}(s)+\cos^2\delta\sin\theta_V(4\cos\theta_V-\sqrt{2}\sin\theta_V)] \\
& -2\sin\theta_P(\cos^2\delta+\sin\delta^{\omega}(Q^2)\sin\delta^{\omega}(s))\Big\}BW_{RR}[\eta,\omega,\omega,Q^2,s]\ D_{R\eta 1}(Q^2,s,m_\eta^2) \\
& -\frac{2F_V(1+8\sqrt{2}\alpha_V\frac{m_\pi^2}{M_V^2})G_V}{3\sqrt{6}F^3}\sin\delta^{\omega}(s)\left(-\sin\delta^{\omega}(Q^2)+\frac{1}{\sqrt{3}}\cos\delta\sin\theta_V\right) \\
& \times\Big\{8\cos^2\delta[\cos\theta_P(-3\sqrt{2}+\sqrt{2}\cos 2\theta_V+4\sin 2\theta_V) \\
& +(-3+\cos 2\theta_V+2\sqrt{2}\sin 2\theta_V)\sin\theta_P]m_K^2 \\
& +[12\sin\delta^{\omega}(Q^2)\sin\delta^{\omega}(s)(\sqrt{2}\cos\theta_P-2\sin\theta_P)
\end{aligned}
$$

JHEP03(2021)092

$$
\begin{aligned}
&+\cos^2\delta(-9\sqrt{2}\cos(2\theta_V-\theta_P)+18\sqrt{2}\cos\theta_P+7\sqrt{2}\cos(2\theta_V+\theta_P)\\
&-8\sin(2\theta_V+\theta_P))]m_\pi^2\Big\}BW_{RR}[\eta,\omega,\omega,Q^2,s]\ D_{R\eta 2}\\
&+\frac{2F_V(1+8\sqrt{2}\alpha_V\frac{m_\pi^2}{M_V^2})G_V}{\sqrt{6}F^3}\cos\delta\left(-\sin\delta^\omega(Q^2)+\frac{1}{\sqrt{3}}\cos\delta\sin\theta_V\right)\\
&\times\Big\{\Big(-\frac{1}{2}\cos^2\theta_V\cos\theta_p\sin\delta^\rho(s)+\frac{1}{2}\sin^2\theta_V\cos\theta_p\sin\delta^\rho(s)\\
&-2\sqrt{2}\sin\theta_V\cos\theta_V\cos\theta_P\sin\delta^\rho(s)+\sqrt{2}\sin\theta_P\sin\delta^\rho(s)\\
&+\frac{1}{2}\cos\theta_P\sin\delta^\rho(s)-\sqrt{2}\sin\theta_P\sin\delta^\omega(Q^2)+\cos\theta_P\sin\delta^\omega(Q^2)\Big)(-4\sqrt{2}\cos\delta)\Big\}\\
&\times BW_{RR}[\eta,\omega,\rho,Q^2,s]\ D_{R\eta 1}(Q^2,s,m_\eta^2)\\
&+\frac{2F_V(1+8\sqrt{2}\alpha_V\frac{m_\pi^2}{M_V^2})G_V}{3\sqrt{6}F^3}\cos\delta\left(-\sin\delta^\omega(Q^2)+\frac{1}{\sqrt{3}}\cos\delta\sin\theta_V\right)\\
&\times BW_{RR}[\eta,\omega,\rho,Q^2,s]\ D_{R\eta 2}\\
&\times\Big\{-\sqrt{2}\cos\delta\ [m_\pi^2(\sin\delta^\rho(s)(4\sqrt{2}\sin(2\theta_V+\theta_P)+9\cos(2\theta_V-\theta_P)-7\cos(2\theta_V+\theta_P)\\
&-18\cos\theta_P)+12\sin\delta^\omega(Q^2)(\cos\theta_P-\sqrt{2}\sin\theta_P))-4m_K^2\sin\delta^\rho(s)\\
&\times(2\cos\theta_P(2\sqrt{2}\sin 2\theta_V+\cos 2\theta_V-3)+\sin\theta_P(4\sin 2\theta_V+\sqrt{2}\cos 2\theta_V-3\sqrt{2}))]\Big\}\\
&-\frac{2F_V(1+8\sqrt{2}\alpha_V\frac{m_\pi^2}{M_V^2})G_V}{\sqrt{6}F^3}\left(\cos\delta+\frac{1}{\sqrt{3}}\sin\delta^\rho(Q^2)\sin\theta_V\right)\\
&\times BW_{RR}[\eta,\rho,\omega,Q^2,s]D_{R\eta 1}(Q^2,s,m_\eta^2)\\
&\times\Big\{-4\sqrt{2}\cos\delta\sin\delta^\omega(s)(\cos\theta_P(\sin\theta_V\sin\delta^\rho(Q^2)(\sin\theta_V-2\sqrt{2}\cos\theta_V)\\
&+\sin\delta^\omega(s))+\sqrt{2}\sin\theta_P(\sin\delta^\rho(Q^2)-\sin\delta^\omega(s)))\Big\}\\
&-\frac{2F_V(1+8\sqrt{2}\alpha_V\frac{m_\pi^2}{M_V^2})G_V}{3\sqrt{6}F^3}\left(\cos\delta+\frac{1}{\sqrt{3}}\sin\delta^\rho(Q^2)\sin\theta_V\right)\\
&\times\Big\{-\sqrt{2}\cos\delta\sin\delta^\omega(s)[m_\pi^2(\sin\delta^\rho(Q^2)(4\sqrt{2}\sin(2\theta_V+\theta_P)+9\cos(2\theta_V-\theta_P)\\
&-7\cos(2\theta_V+\theta_P)-18\cos\theta_P)+12\sin\delta^\omega(s)(\cos\theta_P-\sqrt{2}\sin\theta_P))-4m_K^2\sin\delta^\rho(Q^2)\\
&\times(2\cos\theta_P(2\sqrt{2}\sin 2\theta_V+\cos 2\theta_V-3)+\sin\theta_P(4\sin 2\theta_V+\sqrt{2}\cos 2\theta_V-3\sqrt{2}))]\Big\}\\
&\times BW_{RR}[\eta,\rho,\omega,Q^2,s]\ D_{R\eta 2}\\
&-\frac{4F_V(1+8\sqrt{2}\alpha_V\frac{2{m_K}^2-m_\pi^2}{M_V^2})G_V}{3\sqrt{2}F^3}\cos\delta\cos\theta_V\cos\theta_P\sin\delta^\rho(s)\\
&\times\left(-4\cos 2\theta_V+\sqrt{2}\sin 2\theta_V\right)BW_{RR}[\eta,\phi,\rho,Q^2,s]\ D_{R\eta 1}(Q^2,s,m_\eta^2)\\
&+\frac{4F_V(1+8\sqrt{2}\alpha_V\frac{2m_K^2-m_\pi^2}{M_V^2})G_V}{9\sqrt{2}F^3}
\end{aligned}
$$

JHEP03(2021)092

$$
\begin{aligned}
&\times \cos\delta\cos\theta_V \sin\delta^\rho(s)\Big\{4(2\sqrt{2}\cos 2\theta_V - \sin 2\theta_V)\sin\theta_P(m_K^2 - m_\pi^2)\\
&+ \cos\theta_P(4\cos 2\theta_V - \sqrt{2}\sin 2\theta_V)(4m_K^2 - m_\pi^2)\Big\}\ BW_{RR}[\eta,\phi,\rho,Q^2,s]\ D_{R\eta 2}\\
&+ \frac{4F_V(1+8\sqrt{2}\alpha_V\frac{2m_K^2-m_\pi^2}{M_V^2})G_V}{3\sqrt{2}F^3}\sin\delta^\omega(s)\cos\theta_V\cos\delta\cos\theta_P\\
&\times(-4\cos 2\theta_V + \sqrt{2}\sin 2\theta_V)BW_{RR}[\eta,\phi,\omega,Q^2,s]\ D_{R\eta 1}(Q^2,s,m_\eta^2)\\
&- \frac{4F_V(1+8\sqrt{2}\alpha_V\frac{2{m_K}^2-m_\pi^2}{M_V^2})G_V}{9\sqrt{2}F^3}\sin\delta^\omega(s)\cos\theta_V\cos\delta\\
&\times\Big\{4(2\sqrt{2}\cos 2\theta_V - \sin 2\theta_V)\sin\theta_P(m_K^2 - m_\pi^2) + \cos\theta_P\\
&\times(4\cos 2\theta_V - \sqrt{2}\sin 2\theta_V)(4m_K^2 - m_\pi^2)\Big\}\ BW_{RR}[\eta,\phi,\omega,Q^2,s]\ D_{R\eta 2}.
\end{aligned}
$$

A.2 Decay widths involving vector resonances

A.2.1 Two-body decays

$$
\begin{aligned}
\Gamma_{\omega\to\pi\pi} &= \frac{G_V^2\,M_\omega^3}{48\pi F^4}\sin^2\delta^\omega(M_\omega^2)\left(1-\frac{4m_\pi^2}{M_\omega^2}\right)^{3/2},\\
\Gamma_{\rho\to\ell^+\ell^-} &= \frac{4\,\alpha^2\,\pi\,F_V^2}{3\,M_\rho}\left(1+8\sqrt{2}\alpha_V\frac{m_\pi^2}{M_V^2}\right)^2\left(\cos\delta+\frac{1}{\sqrt{3}}\sin\theta_V\sin\delta^\rho(M_\rho^2)\right)^2\\
&\quad\times\left(1+\frac{2m_\ell^2}{M_\rho^2}\right)\left(1-\frac{4m_\ell^2}{M_\rho^2}\right)^{1/2},\\
\Gamma_{\omega\to\ell^+\ell^-} &= \frac{4\,\alpha^2\,\pi\,F_V^2}{27\,M_\omega}\left(1+8\sqrt{2}\alpha_V\frac{m_\pi^2}{M_V^2}\right)^2(\sqrt{3}\sin\theta_V\cos\delta-3\sin\delta^\omega(M_\omega^2))^2\\
&\quad\times\left(1+\frac{2m_\ell^2}{M_\omega^2}\right)\left(1-\frac{4m_\ell^2}{M_\omega^2}\right)^{1/2},\\
F_{\rho^0\to\pi^0\gamma} &= \frac{2\sqrt{2}}{3M_V F}C_{R\pi}(0,M_\rho^2)\left(\cos\delta+\sqrt{6}\cos\theta_V\sin\delta^\rho(M_\rho^2)+\sqrt{3}\sin\delta^\rho(M_\rho^2)\sin\theta_V\right)\\
&\quad-\frac{4F_V\left(1+8\sqrt{2}\alpha_V\frac{m_\pi^2}{M_V^2}\right)}{3M_\rho^2 F}D_{R\pi}(0,M_\rho^2)(\sin\theta_V\sin\delta^\rho(0)+\sqrt{3}\cos\delta)\\
&\quad\times[\sin\delta^\rho(M_\rho^2)+\sin\delta^\rho(0)]\cos\delta(\sqrt{2}\cos\theta_V+\sin\theta_V)\\
&\quad-\frac{4F_V\left(1+8\sqrt{2}\alpha_V\frac{m_\pi^2}{M_V^2}\right)}{3M_\omega^2 F}D_{R\pi}(0,M_\rho^2)(\sin\theta_V\cos\delta-\sqrt{3}\sin\delta^\omega(0))\\
&\quad\times[\cos^2\delta-\sin\delta^\rho(M_\rho^2)\sin\delta^\omega(0)](\sqrt{2}\cos\theta_V+\sin\theta_V)\\
&\quad-\frac{4F_V\left(1+8\sqrt{2}\alpha_V\frac{2m_K^2-m_\pi^2}{M_V^2}\right)}{3M_\phi^2 F}D_{R\pi}(0,M_\rho^2)\cos\theta_V\cos\delta(\cos\theta_V-\sqrt{2}\sin\theta_V),
\end{aligned}
$$

JHEP03(2021)092

$$
\begin{aligned}
F_{\rho^\pm\to\pi^\pm\gamma} =& \frac{2\sqrt{2}}{3M_V F} C_{R\pi}(0, M_\rho^2) \\
& - \frac{4F_V\left(1+8\sqrt{2}\alpha_V \frac{m_\pi^2}{M_V^2}\right)}{3M_\rho^2 F} D_{R\pi}(0, M_\rho^2) \sin\delta^\rho(0) \\
& \times (\sqrt{2}\cos\theta_V + \sin\theta_V)(\sin\theta_V \sin\delta^\rho(0) + \sqrt{3}\cos\delta) \\
& - \frac{4F_V\left(1+8\sqrt{2}\alpha_V \frac{m_\pi^2}{M_V^2}\right)}{3M_\omega^2 F} D_{R\pi}(0, M_\rho^2) \\
& \times \cos\delta(\sqrt{2}\cos\theta_V + \sin\theta_V)(\sin\theta_V \cos\delta - \sqrt{3}\sin\delta^\omega(0)) \\
& - \frac{4F_V\left(1+8\sqrt{2}\alpha_V \frac{2m_K^2-m_\pi^2}{M_V^2}\right)}{3M_\phi^2 F} D_{R\pi}(0, M_\rho^2) \cos\theta_V(\cos\theta_V - \sqrt{2}\sin\theta_V)\,, \\
F_{\phi\to\pi^0\gamma} =& \frac{2\sqrt{6}}{3M_V F} C_{R\pi}(0, M_\phi^2)(\cos\theta_V - \sqrt{2}\sin\theta_V) \\
& - \frac{4F_V\left(1+8\sqrt{2}\alpha_V \frac{m_\pi^2}{M_V^2}\right)}{3M_\rho^2 F} D_{R\pi}(0, M_\phi^2) \\
& \times (\sin\theta_V \sin\delta^\rho(0) + \sqrt{3}\cos\delta)\cos\delta(\cos\theta_V - \sqrt{2}\sin\theta_V) \\
& - \frac{4F_V\left(1+8\sqrt{2}\alpha_V \frac{m_\pi^2}{M_V^2}\right)}{3M_\omega^2 F} D_{R\pi}(0, M_\phi^2) \\
& \times (\sin\theta_V \cos\delta - \sqrt{3}\sin\delta^\omega(0))\sin\delta^\omega(0)(-\cos\theta_V + \sqrt{2}\sin\theta_V)\,, \\
F_{\omega\to\pi^0\gamma} =& \frac{2\sqrt{2}}{3M_V F} C_{R\pi}(0, M_\omega^2)\left(\sqrt{3}\cos\delta(\sqrt{2}\cos\theta_V + \sin\theta_V) - \sin\delta^\omega(M_\omega^2)\right) \\
& - \frac{4F_V\left(1+8\sqrt{2}\alpha_V \frac{m_\pi^2}{M_V^2}\right)}{3M_\rho^2 F} D_{R\pi}(0, M_\omega^2)(\sin\theta_V \sin\delta^\rho(0) + \sqrt{3}\cos\delta) \\
& \times (\cos^2\delta - \sin\delta^\rho(0)\sin\delta^\omega(M_\omega^2))(\sqrt{2}\cos\theta_V + \sin\theta_V) \\
& + \frac{4F_V\left(1+8\sqrt{2}\alpha_V \frac{m_\pi^2}{M_V^2}\right)}{3M_\omega^2 F} D_{R\pi}(0, M_\omega^2)(\sin\theta_V \cos\delta - \sqrt{3}\sin\delta^\rho(0)) \\
& \times (\sin\delta^\omega(M_\omega^2) + \sin\delta^\omega(0))\cos\delta(\sqrt{2}\cos\theta_V + \sin\theta_V) \\
& - \frac{4F_V\left(1+8\sqrt{2}\alpha_V \frac{2m_K^2-m_\pi^2}{M_V^2}\right)}{3M_\phi^2 F} D_{R\pi}(0, M_\omega^2) \\
& \times \cos\theta_V \sin\delta^\omega(M_\omega^2)(-\cos\theta_V + \sqrt{2}\sin\theta_V)\,, \\
F_{\omega\to\eta\gamma} =& \frac{2\sqrt{2}}{3M_V F} C_{R\eta 1}(0, M_\omega^2, m_\eta^2) \\
& \times \Big\{\sqrt{3}\sin\delta^\omega(M_\omega^2)(-\cos\theta_P + \sqrt{2}\sin\theta_P)
\end{aligned}
$$

JHEP03(2021)092

$$
\begin{aligned}
&+\cos\delta[\sqrt{2}\cos\theta_V\cos\theta_P-\sin\theta_V(\cos\theta_P+\sqrt{2}\sin\theta_P)]\Big\}\\
&+\frac{2\sqrt{2}}{9M_VF}C_{R\eta 2}\Big\{4\cos\delta\left(\sqrt{2}\cos(\theta_V+\theta_P)-2\cos\theta_P\sin\theta_V+\cos\theta_V\sin\theta_P\right)m_K^2\\
&-\Big(3\sqrt{3}\sin\delta^{\omega}(M_\omega^2)(\cos\theta_P-\sqrt{2}\sin\theta_P)\\
&+\cos\delta[\sqrt{2}\cos(\theta_V+\theta_P)-5\cos\theta_P\sin\theta_V+4\cos\theta_V\sin\theta_P]\Big)m_\pi^2\Big\}\\
&-\frac{F_V\left(1+8\sqrt{2}\alpha_V\frac{m_\pi^2}{M_V^2}\right)}{3\sqrt{2}M_\rho^2F}D_{R\eta 1}(0,M_\omega^2,m_\eta^2)(\sin\theta_V\sin\delta^{\rho}(0)+\sqrt{3}\cos\delta)\\
&\times\Big\{(-4\sqrt{2}\cos\delta)\Big(-\frac{1}{2}\cos^2\theta_V\cos\theta_p\sin\delta^{\rho}(0)+\frac{1}{2}\sin^2\theta_V\cos\theta_p\sin\delta^{\rho}(0)\\
&-2\sqrt{2}\sin\theta_V\cos\theta_V\cos\theta_P\sin\delta^{\rho}(0)+\sqrt{2}\sin\theta_P\sin\delta^{\rho}(0)+\frac{1}{2}\cos\theta_P\sin\delta^{\rho}(0)\\
&-\sqrt{2}\sin\theta_P\sin\delta^{\omega}(M_\omega^2)+\cos\theta_P\sin\delta^{\omega}(M_\omega^2)\Big)\Big\}\\
&-\frac{F_V\left(1+8\sqrt{2}\alpha_V\frac{m_\pi^2}{M_V^2}\right)}{9\sqrt{2}M_\rho^2F}D_{R\eta 2}(\sin\theta_V\sin\delta^{\rho}(0)+\sqrt{3}\cos\delta)\\
&\times\Big\{-\sqrt{2}\cos\delta\ [m_\pi^2(\sin\delta^{\rho}(0)(4\sqrt{2}\sin(2\theta_V+\theta_P)+9\cos(2\theta_V-\theta_P)\\
&-7\cos(2\theta_V+\theta_P)-18\cos\theta_P)+12\sin\delta^{\omega}(M_\omega^2)(\cos\theta_P-\sqrt{2}\sin\theta_P))\\
&-4m_K^2\sin\delta^{\rho}(0)(2\cos\theta_P(2\sqrt{2}\sin 2\theta_V+\cos 2\theta_V-3)\\
&+\sin\theta_P(4\sin 2\theta_V+\sqrt{2}\cos 2\theta_V-3\sqrt{2}))]\Big\}\\
&-\frac{2\sqrt{2}F_V\left(1+8\sqrt{2}\alpha_V\frac{m_\pi^2}{M_V^2}\right)}{3M_\omega^2F}D_{R\eta 1}(0,M_\omega^2,m_\eta^2)(\sin\theta_V\cos\delta-\sqrt{3}\sin\delta^{\omega}(0))\\
&\times\Big\{\cos\theta_P[\sqrt{2}\sin\delta^{\omega}(0)\sin\delta^{\omega}(M_\omega^2)+\cos^2\delta\sin\theta_V(4\cos\theta_V-\sqrt{2}\sin\theta_V)]\\
&-2[\sin\delta^{\omega}(0)\sin\delta^{\omega}(M_\omega^2)+\cos^2\delta]\sin\theta_P\Big\}\\
&-\frac{F_V\left(1+8\sqrt{2}\alpha_V\frac{m_\pi^2}{M_V^2}\right)}{9\sqrt{2}M_\omega^2F}D_{R\eta 2}(\sin\theta_V\cos\delta-\sqrt{3}\sin\delta^{\omega}(0))\\
&\times\Big\{8\cos^2\delta\left(\cos\theta_P(-3\sqrt{2}+\sqrt{2}\cos 2\theta_V+4\sin 2\theta_V)\right.\\
&\left.+(-3+\cos 2\theta_V+2\sqrt{2}\sin 2\theta_V)\sin\theta_P\right)m_K^2\\
&+\Big(12\sin\delta^{\omega}(0)\sin\delta^{\omega}(M_\omega^2)(\sqrt{2}\cos\theta_P-2\sin\theta_P)\\
&+\cos^2\delta[-9\sqrt{2}\cos(2\theta_V-\theta_P)+18\sqrt{2}\cos\theta_P\\
&+7\sqrt{2}\cos(2\theta_V+\theta_P)-8\sin(2\theta_V+\theta_P)]\Big)m_\pi^2\Big\}\\
&+\frac{\sqrt{2}F_V\left(1+8\sqrt{2}\alpha_V\frac{2m_K^2-m_\pi^2}{M_V^2}\right)}{3M_\phi^2F}D_{R\eta 1}(0,M_\omega^2,m_\eta^2)
\end{aligned}
$$

JHEP03(2021)092

$$
\begin{aligned}
&\times \Big\{\cos\theta_V \cos\delta \cos\theta_P(-4\cos 2\theta_V + \sqrt{2}\sin 2\theta_V)\Big\} \\
&- \frac{\sqrt{2}F_V\left(1+8\sqrt{2}\alpha_V\frac{2m_K^2-m_\pi^2}{M_V^2}\right)}{9M_\phi^2 F} D_{R\eta 2}\cos\theta_V\cos\delta \\
&\times \Big\{4(2\sqrt{2}\cos 2\theta_V - \sin 2\theta_V)\sin\theta_P(m_K^2-m_\pi^2) \\
&+ \cos\theta_P(4\cos 2\theta_V - \sqrt{2}\sin 2\theta_V)(4m_K^2-m_\pi^2)\Big\}\ , \\
F_{\rho^0\to\eta\gamma} = &\frac{2\sqrt{2}}{3M_V F} C_{R\eta 1}(0,M_\rho^2,m_\eta^2)\Big\{\sqrt{3}\cos\delta(\cos\theta_P - \sqrt{2}\sin\theta_P) \\
&+ \sin\delta^\rho(M_\rho^2)[\sqrt{2}\cos\theta_V\cos\theta_P - \sin\theta_V(\cos\theta_P + \sqrt{2}\sin\theta_P)]\Big\} \\
&+ \frac{2\sqrt{2}}{9M_V F} C_{R\eta 2}\Big\{4\sin\delta^\rho(M_\rho^2)\Big(\sqrt{2}\cos(\theta_V+\theta_P) - 2\cos\theta_P\sin\theta_V \\
&+ \cos\theta_V\sin\theta_P\Big)m_K^2 + \Big(3\sqrt{3}\cos\delta(\cos\theta_P - \sqrt{2}\sin\theta_P) \\
&- \sin\delta^\rho(M_\rho^2)[\sqrt{2}\cos(\theta_V+\theta_P) - 5\cos\theta_P\sin\theta_V + 4\cos\theta_V\sin\theta_P]\Big)m_\pi^2\Big\} \\
&- \frac{2\sqrt{2}F_V\left(1+8\sqrt{2}\alpha_V\frac{m_\pi^2}{M_V^2}\right)}{3M_\rho^2 F} D_{R\eta 1}(0,M_\rho^2,m_\eta^2)(\sin\theta_V\sin\delta^\rho(0) + \sqrt{3}\cos\delta) \\
&\times \Big\{\cos^2\delta(\sqrt{2}\cos\theta_P - 2\sin\theta_P) \\
&+ \sin\delta^\rho(M_\rho^2)\sin\delta^\rho(0)[\cos\theta_P\sin\theta_V(4\cos\theta_V - \sqrt{2}\sin\theta_V) - 2\sin\theta_P]\Big\} \\
&- \frac{F_V\left(1+8\sqrt{2}\alpha_V\frac{m_\pi^2}{M_V^2}\right)}{9\sqrt{2}M_\rho^2 F} D_{R\eta 2}(\sin\theta_V\sin\delta^\rho(0) + \sqrt{3}\cos\delta) \\
&\times \Big\{8\sin\delta^\rho(M_\rho^2)\sin\delta^\rho(0)\Big(\cos\theta_P(-3\sqrt{2} + \sqrt{2}\cos 2\theta_V + 4\sin 2\theta_V) \\
&+(-3+\cos 2\theta_V + 2\sqrt{2}\sin 2\theta_V)\sin\theta_P\Big)m_K^2 + \Big(12\cos^2\delta(\sqrt{2}\cos\theta_P - 2\sin\theta_P) \\
&+ \sin\delta^\rho(M_\rho^2)\sin\delta^\rho(0)[-9\sqrt{2}\cos(2\theta_V-\theta_P) + 18\sqrt{2}\cos\theta_P \\
&+7\sqrt{2}\cos(2\theta_V+\theta_P) - 8\sin(2\theta_V+\theta_P)]\Big)m_\pi^2\Big\} \\
&- \frac{F_V\left(1+8\sqrt{2}\alpha_V\frac{m_\pi^2}{M_V^2}\right)}{3\sqrt{2}M_\omega^2 F} D_{R\eta 1}(0,M_\rho^2,m_\eta^2)(\sin\theta_V\cos\delta - \sqrt{3}\sin\delta^\omega(0)) \\
&\times \Big\{(-4\sqrt{2}\cos\delta)\Big(-\frac{1}{2}\cos^2\theta_V\cos\theta_p\sin\delta^\rho(M_\rho^2) + \frac{1}{2}\sin^2\theta_V\cos\theta_p\sin\delta^\rho(M_\rho^2) \\
&- 2\sqrt{2}\sin\theta_V\cos\theta_V\cos\theta_P\sin\delta^\rho(M_\rho^2) + \sqrt{2}\sin\theta_P\sin\delta^\rho(M_\rho^2) \\
&+ \frac{1}{2}\cos\theta_P\sin\delta^\rho(M_\rho^2) - \sqrt{2}\sin\theta_P\sin\delta^\omega(0) + \cos\theta_P\sin\delta^\omega(0)\Big)\Big\} \\
&- \frac{F_V\left(1+8\sqrt{2}\alpha_V\frac{m_\pi^2}{M_V^2}\right)}{9\sqrt{2}M_\omega^2 F} D_{R\eta 2}(\sin\theta_V\cos\delta - \sqrt{3}\sin\delta^\omega(0)) \\
&\times \Big\{-\sqrt{2}\cos\delta\ [m_\pi^2(\sin\delta^\rho(M_\rho^2)(4\sqrt{2}\sin(2\theta_V+\theta_P) + 9\cos(2\theta_V-\theta_P)
\end{aligned}
$$

JHEP03(2021)092

$$
\begin{aligned}
&- 7\cos(2\theta_V+\theta_P) - 18\cos\theta_P) + 12\sin\delta^\omega(0)(\cos\theta_P - \sqrt{2}\sin\theta_P))\\
&- 4m_K^2\sin\delta^\rho(M_\rho^2)(2\cos\theta_P(2\sqrt{2}\sin 2\theta_V + \cos 2\theta_V - 3)\\
&+ \sin\theta_P(4\sin 2\theta_V + \sqrt{2}\cos 2\theta_V - 3\sqrt{2}))]\Big\}\\
&+ \frac{\sqrt{2}F_V\left(1+8\sqrt{2}\alpha_V\frac{2m_K^2-m_\pi^2}{M_V^2}\right)}{3M_\phi^2F} D_{R\eta 1}(0,M_\rho^2,m_\eta^2)\cos\theta_V\cos\theta_P\sin\delta^\rho(M_\rho^2)\\
&\times(-4\cos 2\theta_V + \sqrt{2}\sin 2\theta_V)\\
&- \frac{\sqrt{2}F_V\left(1+8\sqrt{2}\alpha_V\frac{2m_K^2-m_\pi^2}{M_V^2}\right)}{9M_\phi^2F} D_{R\eta 2}\cos\theta_V\sin\delta^\rho(M_\rho^2)\\
&\times\Big\{4(2\sqrt{2}\cos 2\theta_V - \sin 2\theta_V)\sin\theta_P(m_K^2-m_\pi^2)\\
&+\cos\theta_P(4\cos 2\theta_V - \sqrt{2}\sin 2\theta_V)(4m_K^2-m_\pi^2)\Big\}\ ,\\
F_{\phi\to\eta\gamma} =& \frac{2\sqrt{2}}{3M_VF}C_{R\eta 1}(0,M_\phi^2,m_\eta^2)\Big\{-\sqrt{2}\cos\theta_P\sin\theta_V - \cos\theta_V(\cos\theta_P+\sqrt{2}\sin\theta_P)\Big\}\\
&+ \frac{\sqrt{2}}{9M_VF}C_{R\eta 2}\Big\{-4\Big(3\cos(\theta_V-\theta_P)+\cos(\theta_V+\theta_P)+2\sqrt{2}\sin(\theta_V+\theta_P)\Big)m_K^2\\
&+\Big(9\cos(\theta_V-\theta_P)+\cos(\theta_V+\theta_P)+2\sqrt{2}\sin(\theta_V+\theta_P)\Big)m_\pi^2\Big\}\\
&+ \frac{\sqrt{2}F_V\left(1+8\sqrt{2}\alpha_V\frac{m_\pi^2}{M_V^2}\right)}{3M_\rho^2F} D_{R\eta 1}(0,M_\phi^2,m_\eta^2)(\sin\theta_V\sin\delta^\rho(0)+\sqrt{3}\cos\delta)\\
&\times\cos\theta_P\sin\delta^\rho(0)(-4\cos 2\theta_V+\sqrt{2}\sin 2\theta_V)\\
&- \frac{\sqrt{2}F_V\left(1+8\sqrt{2}\alpha_V\frac{m_\pi^2}{M_V^2}\right)}{9M_\rho^2F} D_{R\eta 2}(\sin\theta_V\sin\delta^\rho(0)+\sqrt{3}\cos\delta)\sin\delta^\rho(0)\\
&\times\Big\{4(2\sqrt{2}\cos 2\theta_V - \sin 2\theta_V)\sin\theta_P(m_K^2-m_\pi^2)\\
&+\cos\theta_P(4\cos 2\theta_V - \sqrt{2}\sin 2\theta_V)(4m_K^2-m_\pi^2)\Big\}\\
&+ \frac{\sqrt{2}F_V\left(1+8\sqrt{2}\alpha_V\frac{m_\pi^2}{M_V^2}\right)}{3M_\omega^2F} D_{R\eta 1}(0,M_\phi^2,m_\eta^2)(\sin\theta_V\cos\delta-\sqrt{3}\sin\delta^\omega(0))\\
&\times\cos\delta\cos\theta_P(-4\cos 2\theta_V+\sqrt{2}\sin 2\theta_V)\\
&- \frac{\sqrt{2}F_V\left(1+8\sqrt{2}\alpha_V\frac{m_\pi^2}{M_V^2}\right)}{9M_\omega^2F} D_{R\eta 2}(\sin\theta_V\cos\delta-\sqrt{3}\sin\delta^\omega(0))\cos\delta\\
&\times\Big\{4(2\sqrt{2}\cos 2\theta_V - \sin 2\theta_V)\sin\theta_P(m_K^2-m_\pi^2)\\
&+\cos\theta_P(4\cos 2\theta_V - \sqrt{2}\sin 2\theta_V)(4m_K^2-m_\pi^2)\Big\}\\
&- \frac{2\sqrt{2}F_V\left(1+8\sqrt{2}\alpha_V\frac{2m_K^2-m_\pi^2}{M_V^2}\right)}{3M_\phi^2F} D_{R\eta 1}(0,M_\phi^2,m_\eta^2)\cos\theta_V
\end{aligned}
$$

JHEP03(2021)092

$$
\begin{aligned}
&\times\Big\{-\cos\theta_V\cos\theta_P(\sqrt{2}\cos\theta_V+4\sin\theta_V)-2\sin\theta_P\Big\}\\
&-\frac{\sqrt{2}F_V\left(1+8\sqrt{2}\alpha_V\frac{2m_K^2-m_\pi^2}{M_V^2}\right)}{9M_\phi^2F}D_{R\eta 2}\cos\theta_V\\
&\times\Big\{(\sqrt{2}\cos\theta_V-2\sin\theta_V)^2(\sqrt{2}\cos\theta_P-2\sin\theta_P)m_\pi^2\\
&-4(\sqrt{2}\cos\theta_V+\sin\theta_V)^2(\sqrt{2}\cos\theta_P+\sin\theta_P)(2m_K^2-m_\pi^2)\Big\}\ ,\\
F_{\eta'\to\omega\gamma}=&\frac{2\sqrt{2}}{3M_VF}C_{R\eta 1}(0,M_\omega^2,m_{\eta'}^2)\Big\{\cos\delta\sin\theta_V(\sqrt{2}\cos\theta_P-\sin\theta_P)\\
&+\sqrt{2}\cos\delta\cos\theta_V\sin\theta_P-\sqrt{3}\sin\delta^\omega(M_\omega^2)(\sqrt{2}\cos\theta_P+\sin\theta_P)\Big\}\\
&+\frac{\sqrt{2}}{9M_VF}C_{R\eta 2}\Big\{4\cos\delta\left(-3\cos(\theta_V-\theta_P)+\cos(\theta_V+\theta_P)+2\sqrt{2}\sin(\theta_V+\theta_P)\right)m_K^2\\
&+\Big(-6\sqrt{3}\sin\delta^\omega(M_\omega^2)(\sqrt{2}\cos\theta_P+\sin\theta_P)\\
&-\cos\delta[-9\cos(\theta_V-\theta_P)+\cos(\theta_V+\theta_P)+2\sqrt{2}\sin(\theta_V+\theta_P)]\Big)m_\pi^2\Big\}\\
&-\frac{F_V\left(1+8\sqrt{2}\alpha_V\frac{m_\pi^2}{M_V^2}\right)}{3\sqrt{2}M_\rho^2F}D_{R\eta 1}(0,M_\omega^2,m_{\eta'}^2)(\sin\theta_V\sin\delta^\rho(0)+\sqrt{3}\cos\delta)\\
&\times\Big\{(-4\sqrt{2}\cos\delta)\{\sin\theta_P[\sin\theta_V\sin\delta^\rho(0)(\sin\theta_V-2\sqrt{2}\cos\theta_V)\\
&+\sin\delta^\omega(M_\omega^2)]+\sqrt{2}\cos\theta_P(\sin\delta^\omega(M_\omega^2)-\sin\delta^\rho(0))\}\Big\}\\
&-\frac{F_V\left(1+8\sqrt{2}\alpha_V\frac{m_\pi^2}{M_V^2}\right)}{9\sqrt{2}M_\rho^2F}D_{R\eta 2}(\sin\theta_V\sin\delta^\rho(0)+\sqrt{3}\cos\delta)\\
&\times\Big\{(-2\sqrt{2}\cos\delta)\{\sin\delta^\rho(0)[2m_K^2\ (\cos\theta_P\ (4\sin 2\theta_V+\sqrt{2}\cos 2\theta_V-3\sqrt{2})\\
&-2\sin\theta_P(2\sqrt{2}\sin 2\theta_V+\cos 2\theta_V-3))+m_\pi^2\ (-2\sqrt{2}\cos(2\theta_V+\theta_P)\\
&-8\sin 2\theta_V\cos\theta_P+(\cos 2\theta_V-9)\sin\theta_P)]+6m_\pi^2\sin\delta^\omega(M_\omega^2)(\sin\theta_P+\sqrt{2}\cos\theta_P)\}\Big\}\\
&-\frac{2\sqrt{2}F_V\left(1+8\sqrt{2}\alpha_V\frac{m_\pi^2}{M_V^2}\right)}{3M_\omega^2F}D_{R\eta 1}(0,M_\omega^2,m_{\eta'}^2)(\sin\theta_V\cos\delta-\sqrt{3}\sin\delta^\omega(0))\\
&\times\Big\{\sin\delta^\omega(M_\omega^2)\times\sin\delta^\omega(0)(2\cos\theta_P+\sqrt{2}\sin\theta_P)\\
&+\cos^2\delta[2\cos\theta_P+\sin\theta_V(4\cos\theta_V-\sqrt{2}\sin\theta_V)\sin\theta_P]\Big\}\\
&-\frac{\sqrt{2}F_V\left(1+8\sqrt{2}\alpha_V\frac{m_\pi^2}{M_V^2}\right)}{9M_\omega^2F}D_{R\eta 2}(\sin\theta_V\cos\delta-\sqrt{3}\sin\delta^\omega(0))\\
&\times\Big\{-4\cos^2\delta\left(\cos\theta_P(-3+\cos 2\theta_V+2\sqrt{2}\sin 2\theta_V)-(-3\sqrt{2}+\sqrt{2}\cos 2\theta_V\right.\\
&\left.+4\sin 2\theta_V)\sin\theta_P\right)m_K^2+\Big(6\sin\delta^\omega(M_\omega^2)\sin\delta^\omega(0)(2\cos\theta_P+\sqrt{2}\sin\theta_P)\\
&+\cos^2\delta\left(4\cos(2\theta_V+\theta_P)+\sqrt{2}[8\cos\theta_P\sin 2\theta_V-(-9+\cos 2\theta_V)\sin\theta_P]\right)\Big)m_\pi^2\Big\}
\end{aligned}
$$

JHEP03(2021)092

$$
\begin{aligned}
&+\frac{\sqrt{2}F_V\left(1+8\sqrt{2}\alpha_V\frac{2m_K^2-m_\pi^2}{M_V^2}\right)}{3M_\phi^2F}D_{R\eta 1}(0,M_\omega^2,m_{\eta'}^2)\\
&\times\Big\{\cos\theta_V\cos\delta(-4\cos 2\theta_V+\sqrt{2}\sin 2\theta_V)\sin\theta_P\Big\}\\
&-\frac{\sqrt{2}F_V\left(1+8\sqrt{2}\alpha_V\frac{2m_K^2-m_\pi^2}{M_V^2}\right)}{9M_\phi^2F}D_{R\eta 2}\cos\theta_V\cos\delta\\
&\times\Big\{-4\cos\theta_P(2\sqrt{2}\cos 2\theta_V-\sin 2\theta_V)(m_K^2-m_\pi^2)\\
&+(4\cos 2\theta_V-\sqrt{2}\sin 2\theta_V)\sin\theta_P(4m_K^2-m_\pi^2)\Big\}\ ,\\
F_{\eta'\to\rho\gamma}=&\frac{2\sqrt{2}}{3M_VF}C_{R\eta 1}(0,M_\rho^2,m_{\eta'}^2)\Big\{\sqrt{3}\cos\delta(\sqrt{2}\cos\theta_P+\sin\theta_P)\\
&+\sin\delta^\rho(M_\rho^2)[\sqrt{2}\cos\theta_P\sin\theta_V+(\sqrt{2}\cos\theta_V-\sin\theta_V)\sin\theta_P]\Big\}\\
&+\frac{\sqrt{2}}{9M_VF}C_{R\eta 2}\Big\{4\sin\delta^\rho(M_\rho^2)\Big(-3\cos(\theta_V-\theta_P)+\cos(\theta_V+\theta_P)\\
&+2\sqrt{2}\sin(\theta_V+\theta_P)\Big)m_K^2+\Big(6\sqrt{3}\cos\delta(\sqrt{2}\cos\theta_P+\sin\theta_P)\\
&-\sin\delta^\rho(M_\rho^2)[-9\cos(\theta_V-\theta_P)+\cos(\theta_V+\theta_P)+2\sqrt{2}\sin(\theta_V+\theta_P)]\Big)m_\pi^2\Big\}\\
&-\frac{2\sqrt{2}F_V\left(1+8\sqrt{2}\alpha_V\frac{m_\pi^2}{M_V^2}\right)}{3M_\rho^2F}D_{R\eta 1}(0,M_\rho^2,m_{\eta'}^2)(\sin\theta_V\sin\delta^\rho(0)+\sqrt{3}\cos\delta)\\
&\times\Big\{\cos^2\delta(2\cos\theta_P+\sqrt{2}\sin\theta_P)\\
&+\sin\delta^\rho(0)\sin\delta^\rho(M_\rho^2)[2\cos\theta_P+\sin\theta_V(4\cos\theta_V-\sqrt{2}\sin\theta_V)\sin\theta_P]\Big\}\\
&-\frac{\sqrt{2}F_V\left(1+8\sqrt{2}\alpha_V\frac{m_\pi^2}{M_V^2}\right)}{9M_\rho^2F}D_{R\eta 2}(\sin\theta_V\sin\delta^\rho(0)+\sqrt{3}\cos\delta)\\
&\times\Big\{-4\sin\delta^\rho(0)\sin\delta^\rho(M_\rho^2)\Big(\cos\theta_P(-3+\cos 2\theta_V+2\sqrt{2}\sin 2\theta_V)\\
&-(-3\sqrt{2}+\sqrt{2}\cos 2\theta_V+4\sin 2\theta_V)\sin\theta_P\Big)m_K^2+\Big(6\cos^2\delta(2\cos\theta_P+\sqrt{2}\sin\theta_P)\\
&+\sin\delta^\rho(0)\sin\delta^\rho(M_\rho^2)\Big(4\cos(2\theta_V+\theta_P)+\sqrt{2}[8\cos\theta_P\sin 2\theta_V\\
&-(-9+\cos 2\theta_V)\sin\theta_P]\Big)\Big)m_\pi^2\Big\}\\
&-\frac{\sqrt{2}F_V\left(1+8\sqrt{2}\alpha_V\frac{m_\pi^2}{M_V^2}\right)}{6M_\omega^2F}D_{R\eta 1}(0,M_\rho^2,m_{\eta'}^2)(\sin\theta_V\cos\delta-\sqrt{3}\sin\delta^\omega(0))\\
&\times\Big\{(-4\sqrt{2}\cos\delta)\{\sin\theta_P[\sin\theta_V\sin\delta^\rho(M_\rho^2)(\sin\theta_V-2\sqrt{2}\cos\theta_V)\\
&+\sin\delta^\omega(0)]+\sqrt{2}\cos\theta_P(\sin\delta^\omega(0)-\sin\delta^\rho(M_\rho^2))\}\Big\}\\
&-\frac{\sqrt{2}F_V\left(1+8\sqrt{2}\alpha_V\frac{m_\pi^2}{M_V^2}\right)}{18M_\omega^2F}D_{R\eta 2}(\sin\theta_V\cos\delta-\sqrt{3}\sin\delta^\omega(0))
\end{aligned}
$$

JHEP03(2021)092

$$
\begin{aligned}
&\times \Big\{(-2\sqrt{2}\cos\delta)\{\sin\delta^\rho(M_\rho^2)[2m_K^2\ (\cos\theta_P\ (4\sin 2\theta_V+\sqrt{2}\cos 2\theta_V-3\sqrt{2})\\
&-2\sin\theta_P(2\sqrt{2}\sin 2\theta_V+\cos 2\theta_V-3))+m_\pi^2\ (-2\sqrt{2}\cos(2\theta_V+\theta_P)\\
&-8\sin 2\theta_V\cos\theta_P+(\cos 2\theta_V-9)\sin\theta_P)]+6m_\pi^2\sin\delta^\omega(0)(\sin\theta_P+\sqrt{2}\cos\theta_P)\Big\}\Big\}\\
&+\frac{\sqrt{2}F_V\left(1+8\sqrt{2}\alpha_V\frac{2m_K^2-m_\pi^2}{M_V^2}\right)}{3M_\phi^2F}D_{R\eta 1}(0,M_\rho^2,m_{\eta'}^2)\\
&\times\Big\{\cos\theta_V\sin\delta^\rho(M_\rho^2)(-4\cos 2\theta_V+\sqrt{2}\sin 2\theta_V)\sin\theta_P\Big\}\\
&-\frac{\sqrt{2}F_V\left(1+8\sqrt{2}\alpha_V\frac{2m_K^2-m_\pi^2}{M_V^2}\right)}{9M_\phi^2F}D_{R\eta 2}\cos\theta_V\sin\delta^\rho(M_\rho^2)\\
&\times\Big\{-4\cos\theta_P(2\sqrt{2}\cos 2\theta_V-\sin 2\theta_V)(m_K^2-m_\pi^2)\\
&+(4\cos 2\theta_V-\sqrt{2}\sin 2\theta_V)\sin\theta_P(4m_K^2-m_\pi^2)\Big\}\ ,\\
F_{\phi\to\eta'\gamma}=&\frac{2\sqrt{2}}{3M_VF}C_{R\eta 1}(0,M_\phi^2,m_{\eta'}^2)\Big\{\sqrt{2}\cos(\theta_V+\theta_P)-\cos\theta_V\sin\theta_P\Big\}\\
&+\frac{\sqrt{2}}{9M_VF}C_{R\eta 2}\Big\{8\Big(\sqrt{2}\cos(\theta_V+\theta_P)+\cos\theta_P\sin\theta_V-2\cos\theta_V\sin\theta_P\Big)m_K^2\\
&+\Big(-2\sqrt{2}\cos(\theta_V+\theta_P)-9\sin(\theta_V-\theta_P)+\sin(\theta_V+\theta_P)\Big)m_\pi^2\Big\}\\
&+\frac{\sqrt{2}F_V\left(1+8\sqrt{2}\alpha_V\frac{m_\pi^2}{M_V^2}\right)}{3M_\rho^2F}D_{R\eta 1}(0,M_\phi^2,m_{\eta'}^2)(\sin\theta_V\sin\delta^\rho(0)+\sqrt{3}\cos\delta)\\
&\times\Big\{\sin\delta^\rho(0)(-4\cos 2\theta_V+\sqrt{2}\sin 2\theta_V)\sin\theta_P\Big\}\\
&-\frac{\sqrt{2}F_V\left(1+8\sqrt{2}\alpha_V\frac{m_\pi^2}{M_V^2}\right)}{9M_\rho^2F}D_{R\eta 2}(\sin\theta_V\sin\delta^\rho(0)+\sqrt{3}\cos\delta)\sin\delta^\rho(0)\\
&\times\Big\{-4\cos\theta_P(2\sqrt{2}\cos 2\theta_V-\sin 2\theta_V)(m_K^2-m_\pi^2)\\
&+(4\cos 2\theta_V-\sqrt{2}\sin 2\theta_V)\sin\theta_P(4m_K^2-m_\pi^2)\Big\}\\
&+\frac{\sqrt{2}F_V\left(1+8\sqrt{2}\alpha_V\frac{m_\pi^2}{M_V^2}\right)}{3M_\omega^2F}D_{R\eta 1}(0,M_\phi^2,m_{\eta'}^2)(\sin\theta_V\cos\delta-\sqrt{3}\sin\delta^\omega(0))\\
&\Big\{\cos\delta(-4\cos 2\theta_V+\sqrt{2}\sin 2\theta_V)\sin\theta_P\Big\}\\
&-\frac{\sqrt{2}F_V\left(1+8\sqrt{2}\alpha_V\frac{m_\pi^2}{M_V^2}\right)}{9M_\omega^2F}D_{R\eta 2}(\sin\theta_V\cos\delta-\sqrt{3}\sin\delta^\omega(0))\cos\delta\\
&\times\Big\{-4\cos\theta_P(2\sqrt{2}\cos 2\theta_V-\sin 2\theta_V)(m_K^2-m_\pi^2)\\
&+(4\cos 2\theta_V-\sqrt{2}\sin 2\theta_V)\sin\theta_P(4m_K^2-m_\pi^2)\Big\}
\end{aligned}
$$

JHEP03(2021)092

$$
\begin{aligned}
&- \frac{2\sqrt{2}F_V\left(1+8\sqrt{2}\alpha_V\frac{2m_K^2-m_\pi^2}{M_V^2}\right)}{3M_\phi^2 F} D_{R\eta 1}(0,M_\phi^2,m_{\eta'}^2)\cos\theta_V \\
&\times\left\{2\cos\theta_P-\cos\theta_V(\sqrt{2}\cos\theta_V+4\sin\theta_V)\sin\theta_P\right\} \\
&- \frac{\sqrt{2}F_V\left(1+8\sqrt{2}\alpha_V\frac{2m_K^2-m_\pi^2}{M_V^2}\right)}{9M_\phi^2 F} D_{R\eta 2}\cos\theta_V \\
&\times\left\{(\sqrt{2}\cos\theta_V-2\sin\theta_V)^2(2\cos\theta_P+\sqrt{2}\sin\theta_P)m_\pi^2\right. \\
&\left.-4(\sqrt{2}\cos\theta_V+\sin\theta_V)^2(-\cos\theta_P+\sqrt{2}\sin\theta_P)(2m_K^2-m_\pi^2)\right\}\,.
\end{aligned}
$$

A.2.2 Three-body decays

The three pion decays of the vector resonances are given by:

$$
\Gamma(V\to\pi^+(p_1)\pi^-(p_2)\pi^0(p_3)) = \frac{1}{256\,\pi^3\,M_V^3}\int_{s_-}^{s_+} ds\int_{t_-}^{t_+} dt\,\mathcal{P}(s,t)|\Omega_V|^2\,, \tag{A.5}
$$

for $V=\rho,\omega,\phi$, where $s=(p_1+p_2)^2$, $t=(p_1+p_3)^2$ and

$$
\mathcal{P}(s,t) = \frac{1}{12}\left[(3m_\pi^2+M_V^2-s)st-st^2-m_\pi^2(m_\pi^2-M_V^2)^2\right]\,. \tag{A.6}
$$

The integration limits are:

$$
\begin{aligned}
s_+ &= (M_V-m_\pi)^2\,,\\
s_- &= 4m_\pi^2\,,\\
t_\mp &= \frac{1}{4s}\left[\left(M_V^2-m_\pi^2\right)^2-\left(\lambda^{1/2}(s,m_\pi^2,m_\pi^2)\pm\lambda^{1/2}(M_V^2,s,m_\pi^2)\right)^2\right]\,.
\end{aligned} \tag{A.7}
$$

Finally Ω_V is defined by

$$
\mathcal{M}_{V\to\pi^+\pi^-\pi^0} = i\varepsilon_{\mu\nu\alpha\beta}\,p_1^\mu\,p_2^\nu\,p_3^\alpha\,\varepsilon_V^\beta\,\Omega_V\,, \tag{A.8}
$$

being ε_V^μ the polarization of the vector meson. Within resonance chiral theory the corresponding reduced amplitudes, Ω_V, are:

$$
\begin{aligned}
\Omega_\omega = &\left(\sqrt{\frac{2}{3}}\cos\theta_V+\sqrt{\frac{1}{3}}\sin\theta_V\right)\frac{8\cos\delta}{M_\omega F^3}\left\{\frac{\sqrt{2}}{M_V}G_{R\pi}(M_\omega^2)\right.\\
&+G_V(\cos^2\delta+\sin\delta^\rho(s)\sin\delta^\omega(M_\omega^2))BW[\rho,s]\;D_{R\pi}(M_\omega^2,s)\\
&+G_V BW[\rho,t]\;D_{R\pi}(M_\omega^2,t)+G_V BW[\rho,u]\;D_{R\pi}(M_\omega^2,u)\\
&\left.+G_V\sin\delta^\omega(M_\omega^2)\,(\sin\delta^\omega(M_\omega^2)\;+\sin\delta^\omega(s)\,)BW[\omega,s]\;D_{R\pi}(M_\omega^2,s)\right\},\\
\Omega_\phi = &\left(\sqrt{\frac{1}{3}}\cos\theta_V-\sqrt{\frac{2}{3}}\sin\theta_V\right)\frac{8}{M_\phi F^3}\left\{\frac{\sqrt{2}}{M_V}G_{R\pi}(M_\phi^2)\right.\\
&+G_V\cos^2\delta\,BW[\rho,s]\;D_{R\pi}(M_\phi^2,s)+G_V BW[\rho,t]\;D_{R\pi}(M_\phi^2,t)\\
&\left.+G_V BW[\rho,u]\;D_{R\pi}(M_\phi^2,u)+G_V\sin^2\delta^\omega(s)\,BW[\omega,s]\;D_{R\pi}(M_\phi^2,s)\right\},
\end{aligned}
$$

JHEP03(2021)092

$$\Omega_\rho = \left(\sqrt{\frac{2}{3}}\cos\theta_V + \sqrt{\frac{1}{3}}\sin\theta_V\right)\frac{8\sin\delta^\rho(M_\rho^2)}{M_\rho F^3}\left\{\frac{\sqrt{2}}{M_V}G_{R\pi}(M_\rho^2)\right.$$
$$+ 2G_V\cos^2\delta\, BW_R[\rho,s]D_{R\pi}(M_\rho^2,s) + G_V BW_R[\rho,t]D_{R\pi}(M_\rho^2,t)$$
$$\left. + G_V BW_R[\rho,u]D_{R\pi}(M_\rho^2,u)\right\} - \left(\sqrt{\frac{2}{3}}\cos\theta_V + \sqrt{\frac{1}{3}}\sin\theta_V\right)$$
$$\times\frac{8\sin\delta^\omega(s)}{M_\rho F^3}G_V(\cos^2\delta - \sin\delta^\rho(M_\rho^2)\sin\delta^\omega(s))\, BW_R[\omega,s]D_{R\pi}(M_\rho^2,s),$$

being $u = M_V^2 + 3m_\pi^2 - s - t$.

References

[1] S. Weinberg, *Phenomenological Lagrangians*, *Physica A* **96** (1979) 327 [INSPIRE].

[2] J. Gasser and H. Leutwyler, *Chiral perturbation theory to one loop*, *Annals phys.* **158** (1984) 142 [INSPIRE].

[3] G. Ecker, J. Gasser, A. Pich and E. de Rafael, *The role of resonances in chiral perturbation theory*, *Nucl. Phys. B* **321** (1989) 311 [INSPIRE].

[4] G. Ecker, J. Gasser, H. Leutwyler, A. Pich and E. de Rafael, *Chiral Lagrangians for massive spin 1 fields*, *Phys. Lett. B* **223** (1989) 425 [INSPIRE].

[5] V. Cirigliano, G. Ecker, M. Eidemuller, R. Kaiser, A. Pich and J. Portoles, *Towards a consistent estimate of the chiral low-energy constants*, *Nucl. Phys. B* **753** (2006) 139 [hep-ph/0603205] [INSPIRE].

[6] J. Portoles, *Basics of resonance chiral theory*, *AIP Conf. Proc.* **1322** (2010) 178 [arXiv:1010.3360] [INSPIRE].

[7] G. 't Hooft, *A planar diagram theory for strong interactions*, *Nucl. Phys. B* **72** (1974) 461 [INSPIRE].

[8] G. 't Hooft, *A two-dimensional model for mesons*, *Nucl. Phys. B* **75** (1974) 461 [INSPIRE].

[9] E. Witten, *Baryons in the* $1/n$ *expansion*, *Nucl. Phys. B* **160** (1979) 57.

[10] M. Knecht and A. Nyffeler, *Resonance estimates of* $O(p^6)$ *low-energy constants and QCD short distance constraints*, *Eur. Phys. J. C* **21** (2001) 659 [hep-ph/0106034] [INSPIRE].

[11] P.D. Ruiz-Femenia, A. Pich and J. Portoles, *Odd intrinsic parity processes within the resonance effective theory of QCD*, *JHEP* **07** (2003) 003 [hep-ph/0306157] [INSPIRE].

[12] V. Cirigliano, G. Ecker, M. Eidemuller, A. Pich and J. Portoles, *The* $\langle$ *VAP* $\rangle$ *Green function in the resonance region*, *Phys. Lett. B* **596** (2004) 96 [hep-ph/0404004] [INSPIRE].

[13] V. Cirigliano, G. Ecker, M. Eidemuller, R. Kaiser, A. Pich and J. Portoles, *The* $\langle$ *SPP* $\rangle$ *Green function and* SU(3) *breaking in K(l3) decays*, *JHEP* **04** (2005) 006 [hep-ph/0503108] [INSPIRE].

[14] T. Husek and S. Leupold, *Two-hadron saturation for the pseudoscalar-vector-vector correlator and phenomenological applications*, *Eur. Phys. J. C* **75** (2015) 586 [arXiv:1507.00478] [INSPIRE].

JHEP03(2021)092

[15] L.-Y. Dai, J. Fuentes-Martín and J. Portolés, *Scalar-involved three-point Green functions and their phenomenology*, *Phys. Rev. D* **99** (2019) 114015 [arXiv:1902.10411] [INSPIRE].

[16] T. Kadavý, K. Kampf and J. Novotny, *OPE of Green functions of chiral currents*, *JHEP* **10** (2020) 142 [arXiv:2006.13006] [INSPIRE].

[17] Z.H. Guo, J.J. Sanz Cillero and H.Q. Zheng, *Partial waves and large N_c resonance sum rules*, *JHEP* **06** (2007) 030 [hep-ph/0701232] [INSPIRE].

[18] M. Jamin, A. Pich and J. Portoles, *What can be learned from the belle spectrum for the decay $\tau^- \to \nu_\tau K_S \pi^-$*, *Phys. Lett. B* **664** (2008) 78 [arXiv:0803.1786] [INSPIRE].

[19] D.G. Dumm, P. Roig, A. Pich and J. Portoles, *Hadron structure in $\tau \to KK\pi\nu_\tau$ decays*, *Phys. Rev. D* **81** (2010) 034031 [arXiv:0911.2640] [INSPIRE].

[20] D.G. Dumm, P. Roig, A. Pich and J. Portoles, *$\tau \to \pi\pi\pi\nu_\tau$ decays and the $a_1(1260)$ off-shell width revisited*, *Phys. Lett. B* **685** (2010) 158 [arXiv:0911.4436] [INSPIRE].

[21] Z.-H. Guo and P. Roig, *One meson radiative tau decays*, *Phys. Rev. D* **82** (2010) 113016 [arXiv:1009.2542] [INSPIRE].

[22] R. Escribano, S. Gonzalez-Solis and P. Roig, *$\tau^- \to K^- \eta^{(\prime)} \nu_\tau$ decays in chiral perturbation theory with Resonances*, *JHEP* **10** (2013) 039 [arXiv:1307.7908] [INSPIRE].

[23] I.M. Nugent, T. Przedzinski, P. Roig, O. Shekhovtsova and Z. Was, *Resonance chiral lagrangian currents and experimental data for $\tau^- \to \pi^-\pi^-\pi^+\nu_\tau$*, *Phys. Rev. D* **88** (2013) 093012 [arXiv:1310.1053] [INSPIRE].

[24] J.A. Miranda and P. Roig, *New τ-based evaluation of the hadronic contribution to the vacuum polarization piece of the muon anomalous magnetic moment*, *Phys. Rev. D* **102** (2020) 114017 [arXiv:2007.11019] [INSPIRE].

[25] Y.-H. Chen, Z.-H. Guo and H.-Q. Zheng, *Study of η-η' mixing from radiative decay processes*, *Phys. Rev. D* **85** (2012) 054018 [arXiv:1201.2135] [INSPIRE].

[26] C.W. Xiao, T. Dato, C. Hanhart, B. Kubis, U.G. Meißner and A. Wirzba, *Towards an improved understanding of $\eta \to \gamma^*\gamma^*$*, arXiv:1509.02194 [INSPIRE].

[27] L.-Y. Dai, X.-W. Kang, U.-G. Meißner, X.-Y. Song and D.-L. Yao, *Amplitude analysis of the anomalous decay $\eta' \to \pi^+\pi^-\gamma$*, *Phys. Rev. D* **97** (2018) 036012 [arXiv:1712.02119] [INSPIRE].

[28] S. Dubinsky, A. Korchin, N. Merenkov, G. Pancheri and O. Shekhovtsova, *Final-state radiation in electron-positron annihilation into a pion pair*, *Eur. Phys. J. C* **40** (2005) 41 [hep-ph/0411113] [INSPIRE].

[29] L.Y. Dai, J. Portoles and O. Shekhovtsova, *Three pseudoscalar meson production in e^+e^- annihilation*, *Phys. Rev. D* **88** (2013) 056001 [arXiv:1305.5751] [INSPIRE].

[30] F. Niecknig, B. Kubis and S.P. Schneider, *Dispersive analysis of $\omega \to 3\pi$ and $\phi \to 3\pi$ decays*, *Eur. Phys. J. C* **72** (2012) 2014 [arXiv:1203.2501] [INSPIRE].

[31] S.P. Schneider, B. Kubis and F. Niecknig, *The $\omega \to \pi^0\gamma^*$ and $\phi \to \pi^0\gamma^*$ transition form factors in dispersion theory*, *Phys. Rev. D* **86** (2012) 054013 [arXiv:1206.3098] [INSPIRE].

[32] I.V. Danilkin et al., *Dispersive analysis of $\omega/\phi \to 3\pi$, $\pi\gamma^*$*, *Phys. Rev. D* **91** (2015) 094029 [arXiv:1409.7708] [INSPIRE].

[33] M. Albaladejo and B. Moussallam, *Extended chiral khuri-Treiman formalism for $\eta \to 3\pi$ and the role of the $a_0(980)$, $f_0(980)$ resonances*, *Eur. Phys. J. C* **77** (2017) 508 [arXiv:1702.04931] [INSPIRE].

JHEP03(2021)092

[34] T. Isken, B. Kubis, S.P. Schneider and P. Stoffer, *Dispersion relations for $\eta' \to \eta\pi\pi$*, *Eur. Phys. J. C* **77** (2017) 489 [arXiv:1705.04339] [INSPIRE].

[35] G. Colangelo, S. Lanz, H. Leutwyler and E. Passemar, *Dispersive analysis of $\eta \to 3\pi$*, *Eur. Phys. J. C* **78** (2018) 947 [arXiv:1807.11937] [INSPIRE].

[36] D.-L. Yao, L.-Y. Dai, H.-Q. Zheng and Z.-Y. Zhou, *A review on partial-wave dynamics with chiral effective field theory and dispersion relation*, arXiv:2009.13495 [INSPIRE].

[37] MUON G-2 collaboration, *Final report of the muon E821 Anomalous magnetic moment measurement at BNL*, *Phys. Rev. D* **73** (2006) 072003 [hep-ex/0602035] [INSPIRE].

[38] PARTICLE DATA GROUP collaboration, *Review of particle physics*, *PTEP* **2020** (2020) 083C01 [INSPIRE].

[39] T. Aoyama et al., *The anomalous magnetic moment of the muon in the Standard model*, *Phys. Rept.* **887** (2020) 1 [arXiv:2006.04822] [INSPIRE].

[40] F. Jegerlehner, *The anomalous magnetic moment of the muon*, Springer, Germany (2017) [INSPIRE].

[41] T. Aoyama, M. Hayakawa, T. Kinoshita and M. Nio, *Complete tenth-order QED Contribution to the muon $g-2$*, *Phys. Rev. Lett.* **109** (2012) 111808 [arXiv:1205.5370] [INSPIRE].

[42] T. Aoyama, T. Kinoshita and M. Nio, *Theory of the anomalous magnetic Moment of the electron*, *Atoms* **7** (2019) 28 [INSPIRE].

[43] R. Jackiw and S. Weinberg, *Weak interaction corrections to the muon magnetic moment and to muonic atom energy levels*, *Phys. Rev. D* **5** (1972) 2396 [INSPIRE].

[44] M. Knecht, S. Peris, M. Perrottet and E. De Rafael, *Electroweak hadronic contributions to the muon $(g-2)$*, *JHEP* **11** (2002) 003 [hep-ph/0205102] [INSPIRE].

[45] A. Czarnecki, W.J. Marciano and A. Vainshtein, *Refinements in electroweak contributions to the muon anomalous magnetic moment*, *Phys. Rev. D* **67** (2003) 073006 [*Erratum ibid.* **73** (2006) 119901] [hep-ph/0212229] [INSPIRE].

[46] C. Gnendiger, D. Stöckinger and H. Stöckinger-Kim, *The electroweak contributions to $(g-2)_\mu$ after the Higgs boson mass measurement*, *Phys. Rev. D* **88** (2013) 053005 [arXiv:1306.5546] [INSPIRE].

[47] J. Prades, E. de Rafael and A. Vainshtein, *The hadronic light-by-light scattering contribution to the muon and electron anomalous magnetic moments*, *Adv. Ser. Direct. High energy phys.* **20** (2009) 303 [arXiv:0901.0306] [INSPIRE].

[48] G. Colangelo, F. Hagelstein, M. Hoferichter, L. Laub and P. Stoffer, *Longitudinal short-distance constraints for the hadronic light-by-light contribution to $(g-2)_\mu$ with large-N_c Regge models*, *JHEP* **03** (2020) 101 [arXiv:1910.13432] [INSPIRE].

[49] I. Danilkin, O. Deineka and M. Vanderhaeghen, *Dispersive analysis of the $\gamma^*\gamma^* \to \pi\pi$ process*, *Phys. Rev. D* **101** (2020) 054008 [arXiv:1909.04158] [INSPIRE].

[50] T. Blum et al., *Connected and leading disconnected hadronic light-by-light contribution to the muon anomalous magnetic moment with a physical pion mass*, *Phys. Rev. Lett.* **118** (2017) 022005 [arXiv:1610.04603] [INSPIRE].

[51] T. Blum et al., *Using infinite volume, continuum QED and lattice QCD for the hadronic light-by-light contribution to the muon anomalous magnetic moment*, *Phys. Rev. D* **96** (2017) 034515 [arXiv:1705.01067] [INSPIRE].

[52] N. Asmussen et al., *Developments in the position-space approach to the HLbL contribution to the muon $g-2$ on the lattice*, PoS(LATTICE2019)195 [arXiv:1911.05573] [INSPIRE].

JHEP03(2021)092

[53] Sz. Borsanyi et al., *Leading hadronic contribution to the muon 2 magnetic moment from lattice QCD*, arXiv:2002.12347.

[54] L.-Y. Dai and M.R. Pennington, *Two photon couplings of the lightest isoscalars from BELLE data*, *Phys. Lett. B* **736** (2014) 11 [arXiv:1403.7514] [INSPIRE].

[55] L.-Y. Dai and M.R. Pennington, *Comprehensive amplitude analysis of* $\gamma\gamma \to \pi^+\pi^-, \pi^0\pi^0$ *and* $\overline{K}K$ *below 1.5 GeV*, *Phys. Rev. D* **90** (2014) 036004 [arXiv:1404.7524] [INSPIRE].

[56] L.-Y. Dai and M.R. Pennington, *Pion polarizabilities from* $\gamma\gamma \to \pi\pi$ *analysis*, *Phys. Rev. D* **94** (2016) 116021 [arXiv:1611.04441] [INSPIRE].

[57] L.-Y. Dai and M.R. Pennington, *Pascalutsa-Vanderhaeghen light-by-light sum rule from photon-photon collisions*, *Phys. Rev. D* **95** (2017) 056007 [arXiv:1701.04460] [INSPIRE].

[58] H. Terazawa, *All the hadronic contributions to the anomalous magnetic moment of the muon and the lamb shift in the hydrogen atom*, *Prog. Theor. Phys.* **39** (1968) 1326 [INSPIRE].

[59] H. Terazawa, *Spectral function of the photon propagator-mass spectrum and timelike form-factors of particles*, *Phys. Rev.* **177** (1969) 2159 [INSPIRE].

[60] M. Davier, A. Hoecker, B. Malaescu and Z. Zhang, *A new evaluation of the hadronic vacuum polarisation contributions to the muon anomalous magnetic moment and to* $\alpha(m_Z^2)$, *Eur. Phys. J. C* **80** (2020) 241 [*Erratum ibid.* **80** (2020) 410] [arXiv:1908.00921] [INSPIRE].

[61] A. Keshavarzi, D. Nomura and T. Teubner, $g-2$ *of charged leptons,* $\alpha(M_Z^2)$ *, and the hyperfine splitting of muonium*, *Phys. Rev. D* **101** (2020) 014029 [arXiv:1911.00367] [INSPIRE].

[62] A. Kurz, T. Liu, P. Marquard and M. Steinhauser, *Hadronic contribution to the muon anomalous magnetic moment to next-to-next-to-leading order*, *Phys. Lett. B* **734** (2014) 144 [arXiv:1403.6400] [INSPIRE].

[63] V.M. Aul'chenko et al., *Study of the* $e^+e^- \to \pi^+\pi^-\pi^0$ *process in the energy range* 1.05–2.00 *GeV*, *J. Exp. Theor. Phys.* **121** (2015) 27 [*Zh. Eksp. Teor. Fiz.* **148** (2015) 34] [INSPIRE].

[64] BESIII collaboration, *Measurement of the* $e^+e^- \to \pi^+\pi^-\pi^0$ *Cross section from* 0.7 *GeV to* 3.0 *GeV via Initial-State radiation*, arXiv:1912.11208 [INSPIRE].

[65] SND collaboration, *Measurement of the* $e^+e^- \to \eta\pi^+\pi^-$ *cross section in the center-of-mass energy range* 1.22–2.00 *GeV with the SND detector at the VEPP-2000 collider*, *Phys. Rev. D* **91** (2015) 052013 [arXiv:1412.1971] [INSPIRE].

[66] M.N. Achasov et al., *Measurement of the* $e^+e^- \to \eta\pi^+\pi^-$ *cross section with the SND detector at the VEPP-2000 collider*, *Phys. Rev. D* **97** (2018) 012008 [arXiv:1711.08862] [INSPIRE].

[67] S.S. Gribanov et al., *Measurement of the* $e^+e^- \to \eta\pi^+\pi^-$ *cross section with the CMD-3 detector at the VEPP-2000 collider*, *JHEP* **01** (2020) 112 [arXiv:1907.08002] [INSPIRE].

[68] BESIII collaboration, *Measurement of the born cross sections for* $e^+e^- \to \eta'\pi^+\pi^-$ *at center-of-mass energies between* 2.00 *and* 3.08 *GeV*, arXiv:2012.07360 [INSPIRE].

[69] BABAR collaboration, *Precise measurement of the* $e^+e^- \to \pi^+\pi^-(\gamma)$ *cross section with the initial-state radiation method at BABAR*, *Phys. Rev. D* **86** (2012) 032013 [arXiv:1205.2228] [INSPIRE].

[70] KLOE collaboration, *Measurement of* $\sigma(e^+e^- \to \pi^+\pi^-\gamma(\gamma)$ *and the dipion contribution to the muon anomaly with the KLOE detector*, *Phys. Lett. B* **670** (2009) 285 [arXiv:0809.3950] [INSPIRE].

JHEP03(2021)092

[71] KLOE collaboration, *Measurement of $\sigma(e^+e^- \to \pi^+\pi^-)$ from threshold to 0.85 GeV^2 using initial state radiation with the KLOE detector*, *Phys. Lett. B* **700** (2011) 102 [arXiv:1006.5313] [INSPIRE].

[72] KLOE collaboration, *Precision measurement of $\sigma(e^+e^- \to \pi^+\pi^-\gamma)/\sigma(e^+e^- \to \mu^+\mu^-\gamma)$ and determination of the $\pi^+\pi^-$ contribution to the muon anomaly with the KLOE detector*, *Phys. Lett. B* **720** (2013) 336 [arXiv:1212.4524] [INSPIRE].

[73] KLOE-2 collaboration, *Combination of KLOE $\sigma\left(e^+e^- \to \pi^+\pi^-\gamma(\gamma)\right)$ measurements and determination of $a_\mu^{\pi^+\pi^-}$ in the energy range $0.10 < s < 0.95$ GeV^2*, *JHEP* **03** (2018) 173 [arXiv:1711.03085] [INSPIRE].

[74] SND collaboration, *Measurement of the $e^+e^- \to \pi^+\pi^-$ process cross section with the SND detector at the VEPP-2000 collider in the energy region $0.525 < \sqrt{s} < 0.883$ GeV*, *JHEP* **01** (2021) 113 [arXiv:2004.00263] [INSPIRE].

[75] BESIII collaboration, *Measurement of the $e^+e^- \to \pi^+\pi^-$ cross section between 600 and 900 MeV using initial state radiation*, *Phys. Lett. B* **753** (2016) 629 [*Erratum ibid.* **812** (2021) 135982] [arXiv:1507.08188] [INSPIRE].

[76] T. Xiao, S. Dobbs, A. Tomaradze, K.K. Seth and G. Bonvicini, *Precision measurement of the hadronic contribution to the muon anomalous magnetic moment*, *Phys. Rev. D* **97** (2018) 032012 [arXiv:1712.04530] [INSPIRE].

[77] CMD-2 collaboration, *Measurement of the pion form-factor in the range 1.04 GeV to 1.38 GeV with the CMD-2 detector*, *JETP Lett.* **82** (2005) 743 [*Pisma Zh. Eksp. Teor. Fiz.* **82** (2005) 841] [hep-ex/0603021] [INSPIRE].

[78] V.M. Aul'chenko et al., *Measurement of the $e^+e^- \to \pi^+\pi^-$ cross section with the CMD-2 detector in the 370–520 MeV c.m. energy range*, *JETP Lett.* **84** (2006) 413 [hep-ex/0610016] [INSPIRE].

[79] CMD-2 collaboration, *High-statistics measurement of the pion form factor in the rho-meson energy range with the CMD-2 detector*, *Phys. Lett. B* **648** (2007) 28 [hep-ex/0610021] [INSPIRE].

[80] DM2 collaboration, *The pion electromagnetic form-factor in the timelike energy range 1.35-{GeV} $\leq \sqrt{s} \leq$ 2.4-{GeV}*, *Phys. Lett. B* **220** (1989) 321 [INSPIRE].

[81] L.M. Barkov et al., *Electromagnetic pion form-factor in the timelike region*, *Nucl. Phys. B* **256** (1985) 365 [INSPIRE].

[82] M.N. Achasov et al., *Measurements of the parameters of the $\phi(1020)$ resonance through studies of the processes $e^+e^- \to K^+K^-$, K_SK_L, and $\pi^+\pi^-\pi^0$*, *Phys. Rev. D* **63** (2001) 072002 [hep-ex/0009036] [INSPIRE].

[83] M.N. Achasov et al., *Measurement of the $e^+e^- \to K^+K^-$ process cross-section in the energy range $\sqrt{s} = 1.04$–1.38 GeV with the SND detector in the experiment at VEPP-2M e^+e^- collider*, *Phys. Rev. D* **76** (2007) 072012 [arXiv:0707.2279] [INSPIRE].

[84] M.N. Achasov et al., *Measurement of the $e^+e^- \to K^+K^-$ cross section in the energy range $\sqrt{s} = 1.05$–2.0 GeV*, *Phys. Rev. D* **94** (2016) 112006 [arXiv:1608.08757] [INSPIRE].

[85] BESIII collaboration, *Measurement of $e^+e^- \to K^+K^-$ cross section at $\sqrt{s} = 2.00$–3.08 GeV*, *Phys. Rev. D* **99** (2019) 032001 [arXiv:1811.08742] [INSPIRE].

[86] BABAR collaboration, *Precision measurement of the $e^+e^- \to K^+K^-(\gamma)$ cross section with the initial-state radiation method at BABAR*, *Phys. Rev. D* **88** (2013) 032013 [arXiv:1306.3600] [INSPIRE].

JHEP03(2021)092

[87] CMD-2 collaboration, *Measurement of $e^+e^- \to \phi \to K^+K^-$ cross section with the CMD-2 detector at VEPP-2M Collider*, *Phys. Lett. B* **669** (2008) 217 [arXiv:0804.0178] [INSPIRE].

[88] E.A. Kozyrev et al., *Study of the process $e^+e^- \to K^+K^-$ in the center-of-mass energy range 1010–1060 MeV with the CMD-3 detector*, *Phys. Lett. B* **779** (2018) 64 [arXiv:1710.02989] [INSPIRE].

[89] E. Witten, *Global aspects of current algebra*, *Nucl. Phys. B* **223** (1983) 422 [INSPIRE].

[90] J. Wess and B. Zumino, *Consequences of anomalous ward identities*, *Phys. Lett. B* **37** (1971) 95 [INSPIRE].

[91] J. Gasser and H. Leutwyler, *Quark masses*, *Phys. Rept.* **87** (1982) 77 [INSPIRE].

[92] E. Arganda, M.J. Herrero and J. Portoles, *Lepton flavour violating semileptonic tau decays in constrained MSSM-seesaw scenarios*, *JHEP* **06** (2008) 079 [arXiv:0803.2039] [INSPIRE].

[93] F. Guerrero and A. Pich, *Effective field theory description of the pion form-factor*, *Phys. Lett. B* **412** (1997) 382 [hep-ph/9707347] [INSPIRE].

[94] A. Pich and J. Portoles, *The vector form-factor of the pion from unitarity and analyticity: a model independent approach*, *Phys. Rev. D* **63** (2001) 093005 [hep-ph/0101194] [INSPIRE].

[95] J.A. Miranda and P. Roig, *Effective-field theory analysis of the $\tau^- \to \pi^-\pi^0\nu_\tau$ decays*, *JHEP* **11** (2018) 038 [arXiv:1806.09547] [INSPIRE].

[96] D. Gomez Dumm, A. Pich and J. Portoles, *The hadronic off-shell width of meson resonances*, *Phys. Rev. D* **62** (2000) 054014 [hep-ph/0003320] [INSPIRE].

[97] A. Cordier et al., *Cross-section of the reaction $e^+e^- \to \pi^+\pi^-\pi^0$ for center-of-mass energies from 750 MeV to 1100 MeV*, *Nucl. Phys. B* **172** (1980) 13.

[98] S.I. Dolinsky et al., *Summary of experiments with the neutral detector at the e^+e^- storage ring VEPP-2M*, *Phys. Rept.* **202** (1991) 99 [INSPIRE].

[99] DM2 collaboration, *Measurement of the $e^+e^- \to \pi^+\pi^-\pi^0$ and $e^+e^- \to \omega\pi^+\pi^-$ reactions in the energy interval 1350 MeV–2400 MeV*, *Z. Phys. C* **56** (1992) 15 [INSPIRE].

[100] CMD-2 collaboration, *Reanalysis of hadronic cross-section measurements at CMD-2*, *Phys. Lett. B* **578** (2004) 285 [hep-ex/0308008] [INSPIRE].

[101] R.R. Akhmetshin et al., *Study of dynamics of $\phi \to \pi^+\pi^-\pi^0$ decay with CMD-2 detector*, *Phys. Lett. B* **434** (1998) 426 [INSPIRE].

[102] CMD-2 collaboration, *Measurement of omega meson parameters in pi+ pi- pi0 decay mode with CMD-2*, *Phys. Lett. B* **476** (2000) 33 [hep-ex/0002017] [INSPIRE].

[103] M.N. Achasov et al., *Study of the process $e^+e^- \to \pi^+\pi^-\pi^0$ in the energy region $\sqrt{s}$ below 0.98 GeV*, *Phys. Rev. D* **68** (2003) 052006 [hep-ex/0305049] [INSPIRE].

[104] M.N. Achasov et al., *Study of the process $e^+e^- \to \pi^+\pi^-\pi^0$ in the energy region $\sqrt{s}$ from 0.98 GeV to 1.38 GeV*, *Phys. Rev. D* **66** (2002) 032001 [hep-ex/0201040] [INSPIRE].

[105] BABAR collaboration, *Study of $e^+e^- \to \pi^+\pi^-\pi^0$ process using initial state radiation with BaBar*, *Phys. Rev. D* **70** (2004) 072004 [hep-ex/0408078] [INSPIRE].

[106] DM2 collaboration, *Measurement of the reaction $e^+e^- \to \eta\pi^+\pi^-$ in the center-of-mass energy interval 1350 MeV to 2400 MeV*, *Phys. Lett. B* **212** (1988) 133 [INSPIRE].

[107] CMD-2 collaboration, *Study of the process $e^+e^- \to \pi^+\pi^-\pi^+\pi^-\pi^0$ with CMD-2 detector*, *Phys. Lett. B* **489** (2000) 125 [hep-ex/0009013] [INSPIRE].

[108] BABAR collaboration, *The $e^+e^- \to 2(\pi^+\pi^-)\pi^0, 2(\pi^+\pi^-)\eta$, $K^+K^-\pi^+\pi^-\pi^0$ and $K^+K^-\pi^+\pi^-\eta$ cross sections measured with initial-State radiation*, *Phys. Rev. D* **76** (2007) 092005 [*Erratum ibid.* **77** (2008) 119902] [arXiv:0708.2461] [INSPIRE].

JHEP03(2021)092

[109] M.N. Achasov et al., *Hadronic cross section measurements at SND*, *Int. J. Mod. Phys. Conf. Ser.* **35** (2014) 1460388 [INSPIRE].

[110] F. James and M. Roos, *Minuit: a system for function minimization and analysis of the parameter errors and correlations*, *Comput. Phys. Commun.* **10** (1975) 343 [INSPIRE].

[111] B. Moussallam, *Chiral sum rules for parameters of the order six Lagrangian in the W-Z sector and application to pi0, eta, eta-prime decays*, *Phys. Rev. D* **51** (1995) 4939 [hep-ph/9407402] [INSPIRE].

[112] B. Moussallam, *A sum rule approach to the violation of Dashen's theorem*, *Nucl. Phys. B* **504** (1997) 381 [hep-ph/9701400] [INSPIRE].

[113] M. Knecht, S. Peris, M. Perrottet and E. de Rafael, *Decay of pseudoscalars into lepton pairs and large N_c QCD*, *Phys. Rev. Lett.* **83** (1999) 5230 [hep-ph/9908283] [INSPIRE].

[114] J. Bijnens, E. Gamiz, E. Lipartia and J. Prades, *QCD short distance constraints and hadronic approximations*, *JHEP* **04** (2003) 055 [hep-ph/0304222] [INSPIRE].

[115] M. Gourdin and E. De Rafael, *Hadronic contributions to the muon g-factor*, *Nucl. Phys. B* **10** (1969) 667 [INSPIRE].

[116] G. Colangelo, M. Hoferichter and P. Stoffer, *Two-pion contribution to hadronic vacuum polarization*, *JHEP* **02** (2019) 006 [arXiv:1810.00007] [INSPIRE].

[117] M. Hoferichter, B.-L. Hoid and B. Kubis, *Three-pion contribution to hadronic vacuum polarization*, *JHEP* **08** (2019) 137 [arXiv:1907.01556] [INSPIRE].

[118] B. Krause, *Higher order hadronic contributions to the anomalous magnetic moment of leptons*, *Phys. Lett. B* **390** (1997) 392 [hep-ph/9607259] [INSPIRE].

JHEP03(2021)092